

# Electron removal processes in proton-methane collisions

Arash Salehzadeh

A THESIS SUBMITTED TO THE FACULTY OF GRADUATE STUDIES IN  
PARTIAL FULFILMENT OF THE REQUIREMENTS FOR THE DEGREE OF  
MASTER OF SCIENCE

GRADUATE PROGRAMME IN THE DEPARTMENT OF PHYSICS AND  
ASTRONOMY

YORK UNIVERSITY

TORONTO ONTARIO

September 2014

©Arash Salehzadeh, 2014.

## Abstract

We have conducted a quantum-mechanical analysis within the independent electron model to investigate electron removal processes in the proton-methane collision system in the 20 keV to a few MeV energy range. Similar to a previous work, we have used a spectral representation of the molecular Hamiltonian and a single-centre expansion of the initially populated molecular orbitals. The two-centre basis generator method is then used to solve the time-dependent single-particle Schrödinger equations. We have also used the “independent atom model” in which we have treated the collision system with a molecular target as a combination of collision systems with atomic targets. We have also shown that Bragg’s additivity rule is derived from the independent atom model.

The results for net capture and ionization cross sections, obtained by the molecular method as well as Bragg’s additivity rule, are compared with available experimental studies. We observe good agreement at high energies for both models. At intermediate and lower energies the situation seems to be less clear. For the molecular method the ionization results are improved when we estimate excitation particularly at intermediate energies. Overall, our molecular method outperforms Bragg’s additivity rule for both capture and ionization.

# Contents

<b>Abstract</b>	<b>ii</b>
<b>Table of Contents</b>	<b>iii</b>
<b>List of Tables</b>	<b>iv</b>
<b>List of Figures</b>	<b>v</b>
<b>1 Introduction</b>	<b>1</b>
<b>2 The Methane molecule</b>	<b>4</b>
2.1 Polyatomic molecules . . . . .	4
2.1.1 Born-Oppenheimer approximation . . . . .	5
2.1.2 Hartree-Fock Method . . . . .	7
2.2 Hartree-Fock treatment of methane . . . . .	11
<b>3 Molecular Two-Centre Basis Generator Method (TC-BGM)</b>	<b>15</b>
3.1 Formulation of the collision dynamics . . . . .	15
3.2 Initial orbitals . . . . .	17
3.3 Collision dynamics . . . . .	21
3.4 Electron removal probabilities . . . . .	22

3.5	Electron removal cross sections . . . . .	24
<b>4</b>	<b>Independent Atom Model</b>	<b>28</b>
4.1	Bragg's additivity rule . . . . .	28
4.2	Independent Atom Model: Procedure . . . . .	31
<b>5</b>	<b>Results</b>	<b>39</b>
5.1	Ionization . . . . .	39
5.1.1	Molecular TC-BGM . . . . .	39
5.1.2	Bragg's rule . . . . .	43
5.1.3	Comparisons . . . . .	45
5.2	Capture . . . . .	48
5.2.1	Molecular TC-BGM . . . . .	48
5.2.2	Bragg's rule . . . . .	49
<b>6</b>	<b>Conclusions</b>	<b>55</b>
	<b>Appendix A Spherical Harmonics</b>	<b>59</b>
	<b>Appendix B Two-centre integrals</b>	<b>62</b>
	<b>Appendix C Expansion Coefficients</b>	<b>63</b>
	<b>Appendix D Molecular Orientations</b>	<b>65</b>
	<b>Appendix E Independent Atom Model</b>	<b>67</b>
E.1	Calculation of Position Vectors . . . . .	67
E.2	Effective Impact Parameters . . . . .	69
	<b>Bibliography</b>	<b>69</b>

# List of Tables

C.1	The expansion coefficients for orthonormalized molecular orbitals . . .	64
-----	---	----

# List of Figures

2.1	Original coordinate system . . . . .	12
3.1	Orientation-dependent net ionization probability as a function of impact parameter (Molecular TC-BGM) . . . . .	26
3.2	Orientation-dependent net capture probability as a function of impact parameter (Molecular TC-BGM) . . . . .	27
4.1	Projection of ( $\alpha = 45, \beta = 90, \gamma = 180$ ) molecular orientation into the azimuthal plane . . . . .	33
4.2	Orientation-dependent net ionization probability as a function of impact parameter (IAM) . . . . .	35
4.3	Orientation-dependent net ionization probability as a function of impact parameter (IAM) . . . . .	36
4.4	The IAM orientation-averaged net capture cross section vs. Bragg's net capture cross sections . . . . .	37
4.5	The IAM orientation-averaged net ionization cross section vs. Bragg's net ionization cross sections . . . . .	38
5.1	Net ionization cross section as a function of impact energy for p-CH <sub>4</sub> with all models included . . . . .	40

5.2	Net ionization cross section as a function of impact energy for p-CH <sub>4</sub> with all models included (logarithmic scale) . . . . .	41
5.3	Net ionization cross section as a function of impact energy for p-CH <sub>4</sub> : Bragg's additivity rule . . . . .	44
5.4	Net ionization cross section as a function of impact energy for p-H <sub>2</sub> : Bragg's additivity rule . . . . .	46
5.5	Ionization cross section as a function of impact energy for p-H . . . .	47
5.6	Net capture cross section as a function of impact energy for p-CH <sub>4</sub> with all models included . . . . .	50
5.7	Net capture cross section as a function of impact energy for p-CH <sub>4</sub> with all models included (logarithmic scale) . . . . .	51
5.8	Net capture cross section as a function of impact energy for p-CH <sub>4</sub> : Bragg's additivity rule . . . . .	53
5.9	Net capture cross section as a function of impact energy for p-H <sub>2</sub> : Bragg's additivity rule . . . . .	54
D.2	The considered molecular orientations . . . . .	66
E.1	Projection of ( $\alpha = 0, \beta = -90, \gamma = -45$ ) molecular orientation into the azimuthal plane . . . . .	69
E.2	Projection of ( $\alpha = 0, \beta = 0, \gamma = -45$ ) molecular orientation into the azimuthal plane . . . . .	70
E.3	Projection of ( $\alpha = -45, \beta = -90, \gamma = 0$ ) molecular orientation into the azimuthal plane . . . . .	71

# Chapter 1

## Introduction

Collisions of ions with hydrocarbon molecular targets have been a subject of interest in both experimental and theoretical physics. The molecule considered in this work is methane,  $\text{CH}_4$ , which is the simplest hydrocarbon molecule. A large number of applications in various fields such as astrophysical and atmospheric sciences has made methane an important molecule to study. One such example is Titan (a satellite of Saturn). Titan's atmosphere is largely composed of  $\text{N}_2$  and hydrocarbon molecules, mainly  $\text{CH}_4$ . The  $\text{CH}_4$  molecules make up about 3% of Titan's atmosphere and are continuously dissociated by UV photons, electrons and cosmic rays [1]. Therefore, studying the dissociation processes of  $\text{CH}_4$  is important in order to understand Titan's atmosphere.

To be able to study the dissociation processes it is essential to understand the simple electron removal processes which precede them. The electron removal and fragmentation processes of hydrocarbon molecules in collisions with different projectiles (i.e., ions, electrons and photons) have been extensively investigated. For example, in [2] the collisions of protons with  $\text{CH}_4$  in the impact energy range of 5-45

keV has been studied experimentally, while in [3, 4, 5, 6] the same collision system has been studied at higher energies (e.g. up to 12 MeV in [4]). However, in [7], in addition to proton projectiles, the collision of anti-protons with CH<sub>4</sub> has been investigated in the impact energy range of 60-5000 keV. Collisions of hydrocarbon targets with electron projectiles have also been studied [8, 9]. In these studies both dissociative and non-dissociative processes have been investigated although the main emphasis has been on dissociative processes. Despite a wide range of experimental studies, however, theoretical studies are scarce and challenging due to the difficulties that arise from the presence of many electrons as well as the multi-centre nature of the CH<sub>4</sub> target.

We have investigated the electron removal processes in p-CH<sub>4</sub> collisions by means of calculating the net ionization and capture cross sections. Net ionization cross sections have been reported in previous experiments [6, 10, 11, 12, 13, 14]. In a more recent paper [15] those cross sections have been combined to yield “recommended data”. Similarly for capture, a number of experiments are available [10, 11, 12, 16, 17, 18, 19, 20] at different impact energies. However, theoretical studies are very limited for this collision system. One theoretical study is presented in [21] where q-fold ionization cross sections in energetic p-CH<sub>4</sub> collisions have been calculated with the continuum distorted wave-eikonal initial state (CDW-EIS) method [22] which is a perturbative approach.

In this work, we present a non-perturbative quantum mechanical analysis of the mentioned collision system in the impact energy range of 20 – 5000 keV. The report is organized in the following way. In chapter (2) we discuss the relevant theoretical concepts. In chapter (3) we present an overview of the properties of the collision system and discuss how the molecular two centre-basis generator method (TC-BGM)

within the independent electron model (IEM) can be used to investigate this problem. In chapter (4) an alternative approach namely the independent atom model (IAM) is explained. Furthermore, in chapter (5) we present our results and compare different models with each other and available experimental results. Chapter (6) contains a summary of our methods and main observations.

## Chapter 2

# The Methane molecule

This chapter mainly deals with the introduction of the wavefunctions for the CH<sub>4</sub> molecule. However, before discussing CH<sub>4</sub> we give a brief overview of the basic concepts of molecular physics.

### 2.1 Polyatomic molecules

The molecular Hamiltonian is (in atomic units where  $\hbar = e = m_e = 4\pi\epsilon_0 = 1$ ):

$$\hat{H} = -\frac{1}{2} \sum_{\alpha} \frac{1}{m_{\alpha}} \nabla_{\alpha}^2 - \frac{1}{2} \sum_i \nabla_i^2 + \sum_{\alpha} \sum_{\beta > \alpha} \frac{Q_{\alpha} Q_{\beta}}{r_{\alpha\beta}} - \sum_{\alpha} \sum_i \frac{Q_{\alpha}}{r_{i\alpha}} + \sum_i \sum_{j > i} \frac{1}{r_{ij}} \quad (2.1)$$

where  $\alpha$  and  $\beta$  are used to label the nuclei while  $i$  and  $j$  are used for the electrons. In the above Hamiltonian the spin-orbit as well as the relativistic interactions are neglected. The first term in (2.1) corresponds to the non-relativistic kinetic energies of the nuclei and, similarly, the second term corresponds to the kinetic energies of the electrons. The third term represents the Coulomb interactions between the nuclei where the internuclear distances are denoted by  $r_{\alpha\beta}$ . The fourth term gives

the Coulomb attraction between the electrons and the nuclei with  $r_{i\alpha}$  being the distance between nucleus  $\alpha$  and electron  $i$ . The last term represents the electron-electron interactions with  $r_{ij}$  being the interelectron distances. Solving the stationary Schrödinger equation for the Hamiltonian (2.1) is not a feasible task which makes it necessary to use approximations. An approximation which is widely used in molecular physics and chemistry is called the Born-Oppenheimer (BO) approximation. The BO approximation is explained in detail in [23, 24, 25, 26]. In the next section we present a brief summary.

### 2.1.1 Born-Oppenheimer approximation

Due to the term  $\sum_{\alpha} \sum_i \frac{Q_{\alpha}}{r_{i\alpha}}$  the Hamiltonian (2.1) cannot be separated into an electronic and a nuclear part. However, according to the BO approximation such a separation is approximately correct. It is based on the fact that the nuclei are much more massive than the electrons and thus the electrons move much faster than the nuclei. Thus, the molecular wavefunction,  $\psi(\vec{r}, \vec{R})$ , ( $\vec{r}$  and  $\vec{R}$  represent the electronic and nuclear coordinates respectively) can be expressed as the product of two functions:

$$\psi(\vec{r}, \vec{R}) = \psi_N(\vec{R})\psi_{el}(\vec{r}, \vec{R}) \quad (2.2)$$

where  $\psi_N(\vec{R})$  is the nuclear wavefunction which depends on the nuclear coordinates while the electronic wavefunction  $\psi_{el}(\vec{r}, \vec{R})$  depends directly on the electronic coordinates and parametrically on the nuclear coordinates. In this notation, spin is suppressed.

Following this separation of the nuclear and electronic motions, one can define

the electronic Hamiltonian as:

$$\hat{H}_{el} = -\frac{1}{2} \sum_i \nabla_i^2 + \sum_{\alpha} \sum_{\beta > \alpha} \frac{Q_{\alpha} Q_{\beta}}{r_{\alpha\beta}} - \sum_{\alpha} \sum_i \frac{Q_{\alpha}}{r_{i\alpha}} + \sum_j \sum_{i > j} \frac{1}{r_{ij}}. \quad (2.3)$$

From the Hamiltonian (2.3) it is evident that  $\psi_{el}$  (which is the solution for the Schrödinger equation for Hamiltonian (2.3) by definition) only depends on the nuclear coordinates through the electrostatic interactions between the nuclei and the electrons as well as the nuclear-nuclear interactions. Thus, it is assumed that the electrons move in an electrostatic field that is generated by the presence of the nuclei. The task is therefore reduced to solving the Schrödinger equation:

$$\hat{H}_{el} \psi_{el}(\vec{r}, \vec{R}) = E_{el}(\vec{R}) \psi_{el}(\vec{r}, \vec{R}). \quad (2.4)$$

Furthermore, one can omit the term  $\sum_{\alpha} \sum_{\beta > \alpha} \frac{Q_{\alpha} Q_{\beta}}{r_{\alpha\beta}}$  from the Hamiltonian (2.3) since it only depends on the nuclear coordinates, and thus is a constant with respect to the electronic coordinates. It can, then, be simply added to the electronic energy at any point.

Therefore, within this approximation, one chooses a nuclear configuration,  $\{\vec{R}\}$  and then solves the electronic Schrödinger equation (2.4) to obtain the energy and the electronic wavefunction  $\psi_{el}$ . By performing the calculations for a set of nuclear configurations it is possible to obtain a configuration which minimizes the energy. In principle, one can also solve a nuclear Schrödinger equation to obtain the nuclear wavefunction  $\psi_N(\vec{R})$  which characterizes vibrational and rotational motion, but for processes such as fast collisions the nuclear motion is unimportant. However, for processes in which the nuclear kinetic energy is comparable to the electrons' kinetic energies the BO approximation is not valid and one has to take other approaches

(e.g. non-adiabatic [24, 27, 28, 29]).

Since the Hamiltonian (2.3) is a many-electron Hamiltonian it is not possible to solve the Schrödinger equation (2.4) exactly and thus one has to use approximations. One of these is the Hartree-Fock (HF) method [23, 30, 31, 32]. A brief introduction to this method is presented in the next section.

### 2.1.2 Hartree-Fock Method

In the HF method one approximates the wavefunctions and the energies of many-body systems. The full many-electron Schrödinger equation is replaced by a set of single-electron orbital equations. The many-electron wavefunction is approximated by a Slater determinant, i.e., one chooses an antisymmetrized product of spin-orbitals to accommodate the Pauli principle:

$$\psi_{el} = \frac{1}{\sqrt{N!}} \begin{vmatrix} \varphi_1(1) & \varphi_2(1) & \dots & \varphi_N(1) \\ \varphi_1(2) & \varphi_2(2) & \dots & \varphi_N(2) \\ \vdots & \vdots & \ddots & \vdots \\ \varphi_1(N) & \varphi_2(N) & \dots & \varphi_N(N) \end{vmatrix}. \quad (2.5)$$

Here we have used a short-hand notation  $\varphi_i(j)$  to express the spin-orbital for the  $j^{th}$  electron. The spin-orbitals  $\varphi_i$  are the products of spatial ( $\phi_i$ ) and spin functions ( $\sigma_i$ ):

$$\varphi_i = \phi_i \sigma_i. \quad (2.6)$$

The ground-state energy is then found by the variational theorem which states:

$$E_{el} = \langle \psi_{el} | \hat{H}_{el} | \psi_{el} \rangle \geq E_{true}. \quad (2.7)$$

The wavefunction that minimizes the energy  $E_{el}$  is, then, the best wavefunction within this approach.

The Hamiltonian (2.3) can be written as the sum of one-electron operators  $h_i$  and two-electron operators  $v_{i,j}$ :

$$\hat{H}_{el} = \sum_i \hat{h}_i + \sum_{j>i} \hat{v}_{ij} \quad (2.8)$$

where

$$\hat{h}_i = -\frac{1}{2}\nabla_i^2 - \sum_{\alpha} \frac{Q_{\alpha}}{r_{i\alpha}} \quad (2.9)$$

and

$$\hat{v}_{ij} = \frac{1}{r_{ij}} \quad (2.10)$$

Accordingly, equation (2.7) can be written as:

$$E_{el} = \sum_{i=1}^N \langle \psi_{el} | \hat{h}_i | \psi_{el} \rangle + \sum_{i=1}^N \sum_{j>1} \langle \psi_{el} | \hat{v}_{ij} | \psi_{el} \rangle \quad (2.11)$$

from which one can derive the following equation:

$$E_{el} = \sum_i^N \langle \phi_i(1) | \hat{h}_1 | \phi_i(1) \rangle + \sum_{i=1}^N \sum_{j>1} (v_{ij}^{coul} - v_{ij}^x) \quad (2.12)$$

where

$$v_{ij}^{coul} = \langle \phi_i(1)\phi_j(2) | \frac{1}{r_{12}} | \phi_i(1)\phi_j(2) \rangle \quad (2.13)$$

is called the Coulomb integral and

$$v_{ij}^x = \langle \phi_i(1)\phi_j(2) | \frac{1}{r_{12}} | \phi_j(1)\phi_i(2) \rangle \quad (2.14)$$

is called the exchange integral.

One finds that the spatial orbitals  $\phi_i$  that minimize the variational integral (2.12) satisfy the HF equation:

$$\hat{F}(1)\phi_i(1) = \epsilon_i\phi_i(1) \quad (2.15)$$

where  $\hat{F}$  is the HF operator:

$$\hat{F}(1) = -\frac{1}{2}\nabla_1^2 - \sum_{\alpha} \frac{Q_{\alpha}}{r_{1\alpha}} + \sum_{j=1}^N (\hat{v}_j^{coul}(1) - \hat{v}_j^x(1)). \quad (2.16)$$

$\hat{v}_j^{coul}$  and  $\hat{v}_j^x$  are the Coulomb and exchange operators respectively, and they are given by:

$$\hat{v}_j^{coul}(1)\phi_i(1) = \phi_i(1) \int |\phi_j(2)|^2 \frac{1}{r_{12}} dv_2 \quad (2.17)$$

and

$$\hat{v}_j^x(1)\phi_i(1) = \phi_j(1) \int \phi_j^*(2)\phi_i(2) \frac{1}{r_{12}} dv_2 \quad (2.18)$$

where the integrals are over all space and spin. Furthermore,  $\epsilon_i$  is:

$$\epsilon_i = \langle \phi_i(1) | \hat{h}_1 | \phi_i(1) \rangle + \sum_{j=1}^N (v_{ij}^{coul} - v_{ij}^x). \quad (2.19)$$

The potential terms in equation (2.16) have the following interpretation: 1) the attraction due to the nuclei (the second term), 2) the average electrostatic repulsion due to all of the electrons, i.e., it is assumed that each electron moves in a charge cloud caused by all of the electrons ( $\hat{v}_j^{coul}$ ). Thus, it is assumed that each electron interacts with itself. 3) This self interaction is corrected by the exchange potential  $\hat{v}_j^x$  for which there is no classical analog and which arises due to the fact that the wavefunctions are chosen to be antisymmetric with respect to electron exchange.

However, the HF method can never yield the exact energy. The reason is that the wavefunction is approximated by a single Slater determinant. The deviation of the HF energy from the true energy is called the correlation energy.

As mentioned previously, the Pauli principle is satisfied in the HF method which means two electrons with the same spin cannot be found at the same place. However, electrons with opposite spin can get too close to each other since their motions are independent of each other. Hence, in this method, electrons with the same spin are correlated and electrons with different spins are not. For this reason, in studies in which the correlation energy is significant the HF method is not an appropriate approach, but improvements can be made by using other methods. One example of an alternative method is density functional theory (DFT) [23, 33] which, in principle, accounts for both exchange and correlation effects. However, in practice, one has to use approximations as well.

Normally, the HF wavefunctions are expanded in terms of a basis and are written as linear combinations of these basis functions. Usually for the molecular HF calculations, the basis functions are atomic functions and thus the molecular orbitals (MOs) are written as linear combinations of atomic orbitals (LCAOs). For example the MOs  $|\phi_i\rangle$  can be expanded in terms of the basis  $\{|\chi_j\rangle\}$  as follows:

$$|\phi_i\rangle = \sum_j C_{ji} |\chi_j\rangle. \quad (2.20)$$

The coefficients  $C_{ji}$  are obtained by the variational method and thus the ones that minimize the energy are chosen. In principle, expansion (2.20) does not involve any approximation, but in practice, the accuracy of the MOs depends on the size of the basis i.e., the larger the basis the more accurate the MOs. However, if the basis is chosen carefully, even a small number of orbitals can yield a good approximation

to the MOs which can save a significant amount of calculation time. In the next section we explain the HF treatment of the CH<sub>4</sub> molecule.

## 2.2 Hartree-Fock treatment of methane

Pitzer [34] has carried out the expansion (2.20) for CH<sub>4</sub> MOs with the AOs being the carbon  $1s, 2s, 2p$  orbitals and a hydrogen  $1s$  for each one of the hydrogen atoms. He has used a minimal basis set i.e., one Slater type orbital (STO) is used for each one of the AOs in each atom. Therefore, in expansion (2.20) the  $\phi_i$  orbitals are the MOs and the  $\{|\chi_j\rangle\}$  basis consists of one STO for each hydrogen and five STOs for the carbon atom. One can also include more STOs for each AO (i.e., use an extended basis set) to improve the accuracy.

STOs have the following form:

$$\chi_{nlm}(r, \theta, \phi) = Nr^{n-1}e^{-Zr}Y_l^m(\theta, \phi) \quad (2.21)$$

where  $N$  is a normalization constant,  $n, l$  and  $m$  are the quantum numbers and  $Z$  is a parameter called orbital exponent.  $Y_l^m$  is a complex spherical harmonic and this form is useful for atomic calculations or diatomic molecules. Complex spherical harmonics are given in appendix (A). However, for the case of polyatomic molecules the real form of the STOs is preferred [23]:

$$\chi'_{nlm}(r, \theta, \phi) = Nr^{n-1}e^{-Zr}Y'_{l,m}(\theta, \phi). \quad (2.22)$$

Thus, we need the spherical harmonics in real form. The real spherical harmonics,  $Y'_{l,m}$ , are explained in appendix (A).

Accordingly, STOs in the real form are used for the carbon  $2p$  orbitals. Thus, the

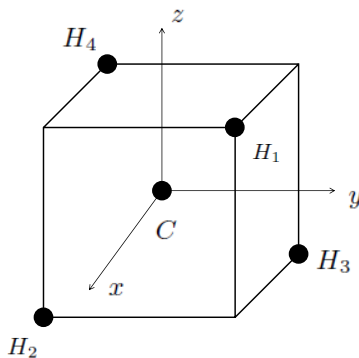


Figure 2.1: The coordinate system used by Pitzer in [23]. The carbon atom is at the origin.

$2p$  AOs on the carbon atom are taken to be  $2p_x$ ,  $2p_y$  and  $2p_z$  rather than  $2p_0$  and the complex-valued  $2p_{\pm 1}$ . They are shown in appendix (A) by equations (A.12), (A.13) and (A.14).

Figure 2.1 shows the coordinate system used in [34] to represent the  $\text{CH}_4$  molecule. The carbon atom is at the origin and the coordinates of the four hydrogen atoms are:  $H_1 = (x, y, z)$ ,  $H_2 = (x, -y, -z)$ ,  $H_3 = (-x, y, -z)$  and  $H_4 = (-x, -y, z)$  where the magnitudes of  $x, y$  and  $z$  are equal and the edge of the cube is  $2x = 2y = 2z$ . The  $\text{CH}_4$  MOs are denoted as  $1a_1$ ,  $2a_1$ ,  $1t_{2x}$ ,  $1t_{2y}$  and  $1t_{2z}$ . This notation refers to the symmetry properties of the MOs. For our purposes, these can be considered as labels.  $1a_1$  is the innermost orbital while the  $1t_{2(x,y,z)}$  orbitals are the degenerate valence orbitals.

The carbon orbitals  $1s$ ,  $2s$ ,  $2p_x$ ,  $2p_y$  and  $2p_z$  have the same symmetry behaviour as the MOs. However, the  $1s$  hydrogen orbitals do not transform according to any of the  $\text{CH}_4$  molecular symmetry species. For this reason, one has to construct symmetry functions that are consistent with the symmetries of the carbon orbitals. This can be achieved by taking appropriate linear combinations of the  $1s$  hydrogen

orbitals as shown in [23]:

$$\chi_1 = H_11s + H_21s + H_31s + H_41s \quad (2.23)$$

$$\chi_2 = H_11s + H_21s - H_31s - H_41s \quad (2.24)$$

$$\chi_3 = H_11s - H_21s + H_31s - H_41s \quad (2.25)$$

$$\chi_4 = H_11s - H_21s - H_31s + H_41s. \quad (2.26)$$

Accordingly, the STOs that Pitzer used for his CH<sub>4</sub> calculations are:  $\chi_1$ ,  $\chi_2$ ,  $\chi_3$ ,  $\chi_4$ ,  $C1s$ ,  $C2s$ ,  $C2p_x$ ,  $C2p_y$ ,  $C2p_z$ . Pitzer's results are shown in detail in [34] for three C-H internuclear distances; 2.00 a.u., 2.05 a.u. and 2.1 a.u. The obtained total energies are  $-40.12568$ ,  $-40.12822$  and  $-40.12698$  hartrees respectively. The energies deduced from experimental studies are  $-40.526$  in [34] and  $-40.515$  hartree in [35]. Thus, the equilibrium C-H distance for which the energy is minimized is taken to be 2.05 a.u. which agrees well with the experimental value of [36]. For the MOs Pitzer found:

$$1a_1 = -0.00468(\chi_1) + 0.9947(C1s) + 0.02561(C2s) \quad (2.27)$$

$$2a_1 = 0.18648(\chi_1) - 0.21584(C1s) + 0.60369(C2s) \quad (2.28)$$

$$1t_{2x} = 0.31779(\chi_2) + 0.55387(C2p_x) \quad (2.29)$$

$$1t_{2y} = 0.31779(\chi_3) + 0.55387(C2p_y) \quad (2.30)$$

$$1t_{2z} = 0.31779(\chi_4) + 0.55387(C2p_z). \quad (2.31)$$

The obtained orbital exponents of  $H_{1s}$ ,  $C_{1s}$ ,  $C_{2s}$  and  $C_{2p}$  are 1.17 a.u., 5.68 a.u., 1.76 a.u. and 1.76 a.u. respectively. The  $1a_1$  orbital and the carbon  $1s$  AO are

essentially the same. The  $2a_1$  orbital has a positive contribution from carbon  $2s$  as well as the four hydrogen atoms and a negative contribution from carbon  $1s$  which is weaker than the  $2s$  contribution. Therefore, there is a charge buildup between the carbon atom and each one of the hydrogen atoms. For  $1t_{2x}$  there is a significant contribution from carbon  $2p_x$  which means there is charge buildup about both the positive and negative sides of the x-axis. The charge buildup gets weaker as we approach  $x = 0$  at which point it vanishes. There is also a charge buildup about  $H_1$  and  $H_2$  (c.f. equation 2.29). Similarly, for  $1t_{2y}$  and  $1t_{2z}$  orbitals there is charge buildup about the y and the z axes respectively.

Other studies have been conducted on  $\text{CH}_4$  by using various methods. Improvements to Pitzer's calculations have been made by using extended basis sets. Woznick [37] has performed similar calculations with an extended STO basis and obtained  $-40.181$  for the energy for bond length of 2.0665. Similarly, for the same value of the bond length Krauss [38] has obtained  $-40.1668$  by using an extended Gaussian type orbitals basis. Different non-variational methods have also been used [35, 39] which take electron correlation into account and yield lower energies than Pitzer's energy.

The above expansions are our starting point for the dynamic calculations. The STO basis is of multi-centre and non-orthogonal nature and, as will be explained in the next chapter, we redo the expansion in an orthonormal, single-centre basis.

## Chapter 3

# Molecular Two-Centre Basis Generator Method (TC-BGM)

### 3.1 Formulation of the collision dynamics

We are considering collisions between protons and  $\text{CH}_4$  molecules in the impact energy range from 20 keV to 5 MeV in which the collisions are sufficiently fast compared with the molecular time scale. Therefore, the molecular rotations and vibrations can be safely neglected. Furthermore, it is assumed that the collision plane is the x-z plane and the projectile follows a classical straight-line trajectory along the z-axis which is characterized by the impact parameter  $\vec{b}$  (the perpendicular distance from the projectile to the z-axis) as well as its velocity  $v$  which is constant.

Due to the presence of electron-electron interactions the full many-electron time dependent Schrödinger equation (TDSE) cannot be solved directly. Hence, we address this problem by using the independent electron model (IEM) in which the

TDSE is approximated by a set of single-electron equations:

$$i\partial_t |\psi_{\alpha\beta\gamma}^\Gamma(t)\rangle = [\hat{H}_{\alpha\beta\gamma}^T + V^P(t)] |\psi_{\alpha\beta\gamma}^\Gamma(t)\rangle \quad (3.1)$$

$$|\psi_{\alpha\beta\gamma}^\Gamma(t_i)\rangle = |\Gamma_{\alpha\beta\gamma}\rangle \quad (3.2)$$

$|\Gamma_{\alpha\beta\gamma}\rangle$  are the initially occupied molecular orbitals (MOs) whose time evolution is studied.  $\alpha, \beta$  and  $\gamma$  are the Euler angles and they specify the molecular orientation with respect to the ion beam axis. We consider the coordinate system shown in figure (2.1) to be the original coordinate system corresponding to the (0, 0, 0) molecular orientation. Other molecular orientations are obtained by rotating this coordinate system by the appropriate Euler angles.  $\hat{H}_{\alpha\beta\gamma}^T$  is the target Hamiltonian and is given by:

$$\hat{H}_{\alpha\beta\gamma}^T = -\frac{1}{2}\nabla^2 + V_{\alpha\beta\gamma}^T \quad (3.3)$$

where  $V_{\alpha\beta\gamma}^T$  is an effective target potential on the HF level.  $V^P(t)$  is the potential that arises from the interaction between the active electron and the projectile.

The solutions of the TDSE (3.1) can be expanded:

$$|\psi_{\alpha\beta\gamma}^\Gamma(t)\rangle = \sum_i a_{i,\alpha\beta\gamma}^\Gamma |\chi_i(t)\rangle. \quad (3.4)$$

The basis  $\{|\chi_i(t)\rangle\}$  can, in general, be a time-dependent, non-orthogonal and a multi-centre basis. If we substitute expansion (3.4) into equation (3.1), a set of coupled channel equations for the expansion coefficients is obtained:

$$i \sum_{j=1} \dot{a}_{j,\alpha\beta\gamma}^\Gamma(t) \langle \chi_k(t) | \chi_j(t) \rangle = \sum_{j=1} a_{j,\alpha\beta\gamma}^\Gamma(t) \langle \chi_k(t) | \hat{H}_{\alpha\beta\gamma}^T + V^P(t) - i\partial_t | \chi_j(t) \rangle. \quad (3.5)$$

The main difficulty of equation (3.5) is the calculation of the multi-centre integrals i.e. the integrals of type  $\langle \chi_k(t) | V_{\alpha\beta\gamma}^T | \chi_j(t) \rangle$ . Therefore, one has to find alternative methods to avoid the explicit calculation of these integrals.

Our approach is based on two ideas: 1) using the spectral representation for the molecular target Hamiltonian

$$\hat{H}_{\alpha\beta\gamma}^T = \sum_{\Lambda} \epsilon_{\Lambda} |\Lambda_{\alpha\beta\gamma}\rangle \langle \Lambda_{\alpha\beta\gamma}| \quad (3.6)$$

where the MOs  $|\Lambda\rangle$  are the molecular target states and  $\epsilon_{\Lambda}$  are the corresponding energy eigenvalues, 2) expanding the MOs in an orthonormal, single-centre basis. The single-centre expansion can only be an accurate approximation for molecules with compact geometries. Since these MOs are orientation dependent, the molecular geometry has to be considered in this expansion. Furthermore, as mentioned previously these orbitals provide the initial conditions for the TDSE solutions. As a result, this calculation is essentially separated into two parts: 1) the molecular geometry problem which deals with calculating the initial conditions for different molecular orientations with respect to the ion beam axis, and 2) the collision dynamics in which the results are propagated in time. In the next section the methods for the expansion of the MOs are presented.

## 3.2 Initial orbitals

Our starting point is the expansion given by Pitzer that was explained in the previous chapter:

$$|\tilde{\Lambda}\rangle = \sum_S C_S^{\Lambda} |S\rangle \quad (3.7)$$

where the calculations have been carried out for the coordinate system in figure (2.1) (our (0,0,0) orientation). The problem with expansion (3.7) is that it leads to complicated multi-centred integrals since the STOs are centred on different atoms. Furthermore, STOs are not orthogonal. For our purposes, a single-centred basis that represents the initially populated MOs is preferable. Hence, we project equation (3.7) onto such a basis:

$$|\Lambda\rangle \equiv \hat{P} |\tilde{\Lambda}\rangle = \sum_{nlm} \langle \varphi_{nlm} | \tilde{\Lambda} \rangle |\varphi_{nlm}\rangle. \quad (3.8)$$

The  $|\varphi_{nlm}\rangle$  orbitals are the eigenstates of the atomic carbon problem and are centred on the carbon atom. They are obtained from the optimized potential method (OPM) of DFT which is often considered to be equivalent to HF (i.e., exchange is treated exactly, but correlation effects are neglected [33, 40]).

From (3.8) we have:

$$|\Lambda\rangle = \sum_{nlm} d_{nlm}^{\Lambda} |\varphi_{nlm}\rangle \quad (3.9)$$

where:

$$d_{nlm}^{\Lambda} = \langle \varphi_{nlm} | \Lambda \rangle = \sum_S C_S^{\Lambda} \langle \varphi_{nlm} | S \rangle. \quad (3.10)$$

To calculate the expansion coefficients  $d_{nlm}^{\Lambda}$  one has to compute the overlap integrals between the OPM orbitals and the STOs ( $|\varphi_{nlm}\rangle$  and  $|S\rangle$ ). Recall that the OPM orbitals are centred on the carbon atom whereas the STOs are centred on both the carbon atom and the hydrogen atoms. Hence, these overlap integrals involve calculating one-centre and two-centre integrals. The method for calculating the two-centre integrals is shown in appendix (B).

Expansion (3.9) has been done for the initial molecular orientation. However, we

have to consider other orientations. To obtain the coefficients for a new orientation a rotated basis has to be introduced:

$$|\tilde{\varphi}_{nlm}\rangle = \hat{R}(\alpha, \beta, \gamma) |\varphi_{nlm}\rangle \quad (3.11)$$

where  $\hat{R}$  is a rotation operator. The MOs can be expanded into the new basis:

$$|\Lambda\rangle = \sum_{nlm} D_{nlm}^{\Lambda}(\alpha, \beta, \gamma) |\tilde{\varphi}_{nlm}\rangle \quad (3.12)$$

where

$$D_{nlm}^{\Lambda}(0, 0, 0) = d_{nlm}^{\Lambda}. \quad (3.13)$$

We are interested in orientations in which the system remains unchanged under a reflection about the y-axis. Such a symmetry corresponds to orientations in which two of the hydrogen atoms are in the collision plane (x-z) with the other two being the mirror images with respect to this plane. Four orientations provide this symmetry behaviour and they are  $(\alpha, \beta, \gamma) = (0, -90, -45)$ ,  $(0, 0, -45)$ ,  $(45, 90, 180)$  and  $(-45, -90, 0)$ . The expansion coefficients for  $(0, -90, -45)$  are shown in the appendix (C) for illustration. Also the molecular orientations in the collision plane are shown in appendix (D). The MOs will either have an even symmetry with respect to this reflection or an odd symmetry. The even orbitals are the gerade,  $g$ , orbitals and the odd ones are the ungerade,  $u$ , orbitals (c.f. appendix (A)). This means that the  $g$  MOs are expanded in terms of the atomic OPM states with the same symmetry behaviour and the  $u$  orbitals likewise. The  $g$  MOs are  $\{ 1a_1, 2a_1, 1t_{2x}$  and  $1t_{2z} \}$

and  $1t_{2y}$  is the only  $u$  MO. Expansion (3.12) can then be expressed as:

$$|\Lambda_{\alpha\beta\gamma}\rangle = \sum_{nlm} D_{g,nlm}^{\Lambda}(\alpha, \beta, \gamma) |\tilde{\varphi}_{g,nlm}\rangle + \sum_{nlm} D_{u,nlm}^{\Lambda}(\alpha, \beta, \gamma) |\tilde{\varphi}_{u,nlm}\rangle \quad (3.14)$$

where the following holds for any given orientation:

$$D_{u,nlm}^{1a_1} = D_{u,nlm}^{2a_1} = D_{u,nlm}^{1t_{2x}} = D_{u,nlm}^{1t_{2z}} = D_{g,nlm}^{1t_{2y}} = 0. \quad (3.15)$$

The non-zero expansion coefficients are:

$$D_{g,nlm}^{\Lambda} = \sum_M d_{g,nlM}^{\Lambda} \langle \varphi_{g,nlm} | \hat{R}(-\gamma, -\beta, -\alpha) | \varphi_{g,nlM} \rangle \quad (3.16)$$

$$+ \sum_M d_{u,nlM}^{\Lambda} \langle \varphi_{g,nlm} | \hat{R}(-\gamma, -\beta, -\alpha) | \varphi_{u,nlM} \rangle \quad (3.17)$$

and

$$D_{u,nlm}^{\Lambda} = \sum_M d_{u,nlM}^{\Lambda} \langle \varphi_{u,nlm} | \hat{R}(-\gamma, -\beta, -\alpha) | \varphi_{u,nlM} \rangle \quad (3.18)$$

$$+ \sum_M d_{g,nlM}^{\Lambda} \langle \varphi_{u,nlm} | \hat{R}(-\gamma, -\beta, -\alpha) | \varphi_{g,nlM} \rangle \quad (3.19)$$

respectively.  $\langle \varphi_{(g/u),nlm} | \hat{R}(-\gamma, -\beta, -\alpha) | \varphi_{(g/u),nlM} \rangle$  can be written in terms of Wigner matrices,  $d_{m,\pm M}^l$ . Finally, the MOs (3.14) are orthonormalized.

Expansion (3.12), thus, provides an expansion of the initial MOs in a single-centre and orthonormal basis. The MOs are then propagated in time as shown in the next section.

### 3.3 Collision dynamics

As mentioned in the previous sections, the aim is to avoid the multi-centre integrals of type  $\langle \chi_k(t) | \hat{H}_{\alpha\beta\gamma}^T | \chi_j(t) \rangle$ . For that reason, we introduced the spectral representation of the target Hamiltonian and obtained an expansion for the MOs in terms of a single-centre, orthonormal basis. Using these ingredients we obtain the following:

$$\langle \chi_k(t) | \hat{H}_{\alpha\beta\gamma}^T | \chi_j(t) \rangle = \sum_{\Lambda} \sum_{s,s'} \epsilon_{\Lambda} \langle \chi_k(t) | s \rangle D_s^{\Lambda}(\alpha, \beta, \gamma) D_{s'}^{\Lambda}(\alpha, \beta, \gamma) \langle s' | \chi_j(t) \rangle \quad (3.20)$$

where we have introduced the following short-hand notation:

$$|\varphi_{nlm}\rangle = |s\rangle \quad (3.21)$$

in which  $s$  is a multi-index.

Thus, we turn the multi-centre integrals into simpler overlap matrix elements by substituting equation (3.20) into the coupled channel equations (3.5). If we use the  $|s\rangle$  states as the initial conditions and solve the set of coupled channel equations we obtain:

$$|\psi_{\alpha\beta\gamma}^s(t)\rangle = \sum_j a_{j,\alpha\beta\gamma}^s(t) |\chi_j(t)\rangle. \quad (3.22)$$

These orbitals can then be combined to reconstruct the molecular solutions,

$$|\psi_{\alpha\beta\gamma}^{\Gamma}(t)\rangle = \sum_s D_{s,\alpha\beta\gamma}^{\Gamma} |\psi_{\alpha\beta\gamma}^s(t)\rangle = \sum_{sj} D_{s,\alpha\beta\gamma}^{\Gamma} a_{j,\alpha\beta\gamma}^s(t) |\chi_j(t)\rangle \quad (3.23)$$

where the sum over  $s$  runs over all of the atomic target states ( $T$ ) that are used to represent the MOs according to equation (3.9). In principle, this approach can give exact solutions within the IEM. However, in practice, all the mentioned expansions

are finite and hence, the solutions are not exact. Three expansions were used: 1) The spectral representation of the molecular Hamiltonian (3.6) where, in principle, an infinite number of bound and continuum states have to be included for an exact treatment. However, we have included only five occupied MOs ( $1a1$ ,  $2a1$ ,  $1t_{2x}$ ,  $1t_{2y}$  and  $1t_{2z}$ ). 2) The expansion of the MOs into the OPM carbon orbitals. 3) The propagation (3.22). For the latter, we have constructed the basis by using the two-centre basis generator method (TC-BGM) which is a two-centre extension of the BGM [41]. The core idea of this approach is to achieve basis set convergence without having to construct a very large basis. A hierarchy of states is generated from a finite set of bound target-centred states by applying a regularized potential centred on the projectile to them recursively. The generated pseudostates represent the continuum and have overlap with bound projectile states. Although the original version of the BGM has shown success in a number of applications, it suffers from the fact that the projectile states are not included in the basis explicitly and thus its applicability to electron capture processes is limited. The TC-BGM basis, however, includes projectile states as well as some target states and the pseudostates. The TC-BGM is explained in more detail in [42]. In this work, the basis includes the target atomic states of the  $KLM$  shells and hydrogen eigenstates of the  $KLMN$  shells for the projectile as well as 41 pseudostates to represent the continuum.

The solutions of the TDSE are used to calculate various observables namely electron capture and ionization cross sections. This is explained in the next section.

### 3.4 Electron removal probabilities

The first step to calculate the electron removal cross sections is to obtain the single particle amplitudes for state-to-state transitions at the final time  $t_f$ . The amplitudes

are obtained by considering the overlap integrals of the propagated orbitals with the final states. The final states include the bound projectile and target states. For the transition to projectile states the amplitude is:

$$A_{if}^P(t_f) = \langle p | \psi_{\alpha\beta\gamma}^\Gamma(t_f) \rangle = \sum_s^T D_{s,\alpha\beta\gamma}^\Gamma a_{p,\alpha\beta\gamma}^s(t_f) \quad (3.24)$$

where the  $|p\rangle$  states are the projectile states. Electron capture probabilities can be found from the projectile amplitude (3.24). We are interested in the total (net) capture and ionization probabilities. For net probabilities one has to consider the contributions from all of the electrons. For the net capture probability we simply consider the electrons in all the projectile states:

$$P_{cap} = \sum_{i=1}^N \sum_f^P |A_{if}^P|^2 \quad (3.25)$$

where  $f$  represents the final projectile states.

Similarly to find the net ionization probability we, first, find the target transition amplitudes:

$$A_{if}^T(t_f) = \langle \Lambda_{\alpha\beta\gamma} | \psi_{\alpha\beta\gamma}^\Gamma(t_f) \rangle = \sum_{s,t}^T D_{t,\alpha\beta\gamma}^\Lambda D_{s,\alpha\beta\gamma}^\Gamma a_{t,\alpha\beta\gamma}^s(t_f) \quad (3.26)$$

where for the final states the bound molecular target orbitals have been considered. Equation (3.26) calculates the transition amplitude to the molecular ground state only and no excited state is considered. Alternatively, one can consider the following for the target transition amplitude:

$$A_{if}^T(t_f) = \sum_s^T D_{s,\alpha\beta\gamma}^\Gamma a_{t,\alpha\beta\gamma}^s(t_f). \quad (3.27)$$

Equation (3.27) considers all of the *KLM* shell atomic target states regardless of whether or not they contribute to the MO ground state.

Due to the unitarity of the problem the electrons that are neither found in the projectile nor in the target are considered to be ionized. Therefore, the net ionization probability is given by:

$$P_{ion} = N - P_{cap} - \sum_{i=1}^N \sum_f^T |A_{if}^T|^2 \quad (3.28)$$

where in this case  $f$  represents the final target states. If equation (3.26) is used to compute the target amplitude then the sum,  $\sum_f^T |A_{if}^T|^2$ , goes over the five molecular target states considered. Therefore, the electrons that are neither bound to the molecular target ground state nor the projectile are considered ionized i.e., target excitation is completely neglected. On the other hand, if equation (3.27) is used, the sum goes over all the atomic target states. This implies that as long as the electrons are in any of the atomic target states they are considered bound to the target. Hence, in this approach, excitation is approximated. As a result, ionization will be weaker due to excitation. This approximation, although being crude, provides an estimate of how significant excitation might be.

### 3.5 Electron removal cross sections

The net electron removal probabilities of equations (3.25) and (3.28) are used to find the corresponding net cross sections. These cross sections, similar to the probabilities, depend on the orientation. For a given orientation the cross section is obtained in the following manner:

$$\sigma_{\alpha\beta\gamma} = \int P_{\alpha\beta\gamma}(\vec{b}) d\vec{b}. \quad (3.29)$$

Experimentally, however, molecules have random orientations i.e., the molecular orientation is not controlled in a typical experiment. Our goal is, therefore, to find cross sections that are orientation averaged in order to be able to compare our results with experimental studies.

If the probabilities were completely independent of orientation (similar to an ion-atom collision), equation (3.29) would become:

$$\sigma = \int P(b)d\vec{b} = 2\pi \int_0^{\infty} bP(b)db \quad (3.30)$$

However, in general, this is not true in the case of molecular targets. Depending on the sensitivity of the system to the molecular orientations the following might serve as an accurate approximation:

$$P_{avg}(b) = \frac{1}{N}(P_{\alpha_1\beta_1\gamma_1} + P_{\alpha_2\beta_2\gamma_2} + \dots + P_{\alpha_N\beta_N\gamma_N}) \quad (3.31)$$

$$\sigma_{avg} = \int P_{avg}(b)d\vec{b} = 2\pi \int_0^{\infty} bP_{avg}(b)db. \quad (3.32)$$

According to this approximation one considers only a few orientations, averages the probabilities and then finds an orientation averaged cross section. One needs to compare the net probabilities for the individual orientations first, to check whether or not this approximation is valid. If different orientations yield very different results this would be a crude (or even a wrong) approximation.

Figures (3.1) and (3.2) show the net ionization and capture probabilities as functions of impact parameter at three impact energies; 20 keV, 50 keV and 500 keV for the four orientations that were considered. It is evident that the system shows a lack of sensitivity toward the molecular orientation particularly at higher energies.

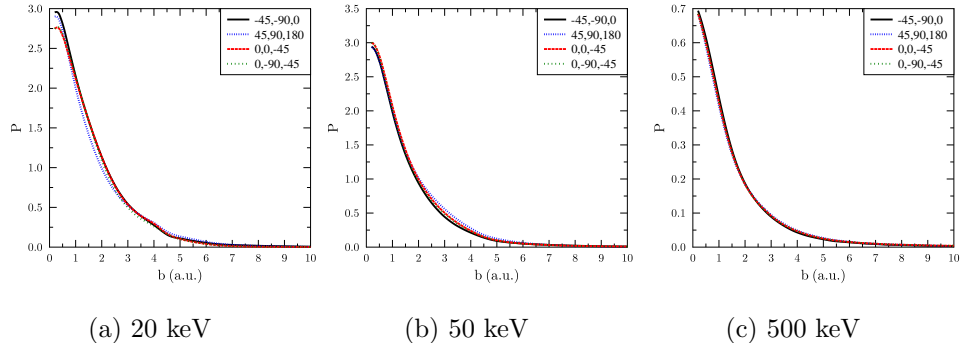


Figure 3.1: Net ionization probability as a function of impact parameter at impact energies: 20 keV, 50 keV and 500 keV. The considered orientations are:  $(\alpha, \beta, \gamma) = (0, -45, -90), (0, 0, -45), (45, 90, 180)$  and  $(-45, -90, 0)$ .

For capture more orientation dependency is observed at low impact parameters for 20 and 50 keV compared to ionization, but at 500 keV there is barely any difference between the four orientations for either capture or ionization. The overall behaviour of the electron removal probabilities suggests that they don't depend on the molecular orientation strongly and hence, equation (3.32) should provide an accurate approximation. Therefore, we have used equations (3.31) (where  $N = 4$ ) and (3.32) to calculate the orientation-averaged cross sections.

Strictly speaking, the results shown in figures (3.1) and (3.2) cannot be conclusive about the low orientation dependency, although they are good indicators. In our molecular calculations, due to symmetry reasons, we were limited to the four mentioned orientations whereas in reality there is an infinite number of them. One might, however unlikely, find other orientations that yield significantly different probabilities. In that case, our calculated average cross section would be inaccurate and we would have to consider more orientations. For that reason, we have further investigated the sufficiency of these four orientations by using the “independent

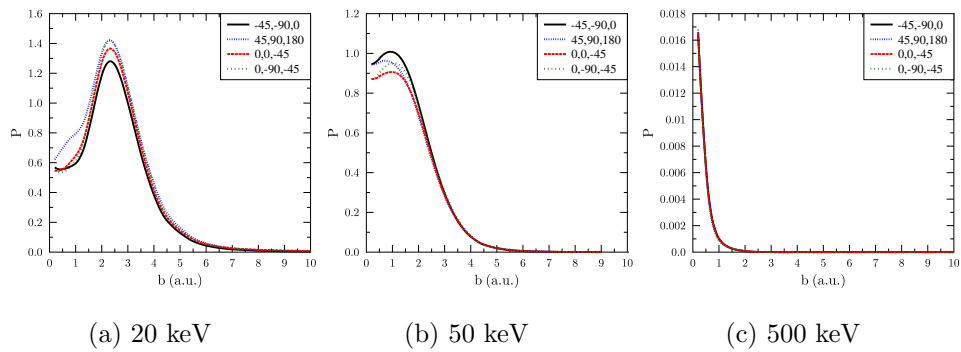


Figure 3.2: Net capture probability as a function of impact parameter at impact energies: 20 keV, 50 keV and 500 keV. The considered orientations are:  $(\alpha, \beta, \gamma) = (0, -45, -90), (0, 0, -45), (45, 90, 180)$  and  $(-45, -90, 0)$ .

atom model” in which the molecule is treated as a collection of individual atoms. Each atom is studied separately and the corresponding atomic results are combined to yield the molecular results. This model is discussed in the next chapter.

## Chapter 4

# Independent Atom Model

### 4.1 Bragg's additivity rule

In addition to the molecular calculations (c.f. chapter (3)) we have used the independent atom model (IAM) to investigate the collision system. In the IAM an ion-molecule collision system is treated as the combination of ion and the individual atom collisions. Thus, the individual atomic net probabilities are combined to yield the net cross sections:

$$\sigma_{\alpha\beta\gamma} = \int P_{\alpha\beta\gamma}(\vec{b}) d\vec{b} \quad (4.1)$$

$$= \sum_i \int P_i(\vec{b}_i) d\vec{b} \quad (4.2)$$

where, as before,  $\vec{b}$  represents the impact parameter vector with respect to the molecular centre (i.e., the carbon atom). Each atom has its own effective impact parameter,  $\vec{b}_i$ , which directly depends on the molecular orientation.

$$\vec{b}_i = \vec{b}_i(\vec{b}, \alpha\beta\gamma). \quad (4.3)$$

In the next section, the method to obtain the individual effective impact parameters is explained.

The relative position in the azimuthal (x-y) plane of each hydrogen atom with respect to the molecular centre is given by:

$$\vec{x}_i = \vec{b} - \vec{b}_i \quad (4.4)$$

and therefore, the two impact parameter vectors are related to each other linearly. Thus:

$$d\vec{b} = d\vec{b}_i. \quad (4.5)$$

We can, then, use equation (4.5) to rewrite equation (4.2) in the following way:

$$\sum_i \int P_i(\vec{b}_i) d\vec{b} = \sum_i \int P_i(\vec{b}_i) d\vec{b}_i = \sum_i \int P_i(\vec{b}) d\vec{b}. \quad (4.6)$$

Since each ion-atom collision is orientation independent we can write equation (4.1) as:

$$\sigma_{\alpha\beta\gamma} = 2\pi \sum_i \int_0^\infty b P_i(b) db \quad (4.7)$$

$$= \sum_i \sigma_i. \quad (4.8)$$

Hence, the net cross sections are orientation-independent. Equation (4.8) is Bragg's additivity rule which states that the net cross section for electron removal processes for a given molecule is the sum of the atomic ones. For example, in the case of CH<sub>4</sub>,

the molecular net cross section (for either capture or ionization) would be:

$$\sigma_{CH_4} = \sigma_c + 4\sigma_H. \quad (4.9)$$

Bragg's additivity rule has been tested previously for various collisions at different impact energies [43, 44, 45, 46, 47, 48, 49]. It has been observed in [43] that at low energies it has significant shortcomings for electron capture and its validity should be doubted. The argument is that at low energies the molecular structure becomes important and should be taken into account which is not the case with the simple additivity rule. At higher energies, however, the rule seems to be more applicable although the success is varied.

However, the electron removal probabilities are not independent of molecular orientation. Within the IAM we study the orientation-dependent probabilities. This allows one to extend Bragg's rule to study more detailed cross sections namely charge-state correlated cross sections. For a  $k$ -fold capture and an  $l$ -fold ionization the charge-state correlated probabilities are given by:

$$P_{kl}(\vec{b}, \alpha\beta\gamma) = \sum_{k_1, \dots, k_5} \sum_{l_1, \dots, l_5} P_{k_1 l_1}^C(\vec{b}_1) P_{k_2 l_2}^{H_1}(\vec{b}_2) P_{k_3 l_3}^{H_2}(\vec{b}_3) P_{k_4 l_4}^{H_3}(\vec{b}_4) P_{k_5 l_5}^{H_4}(\vec{b}_5) \quad (4.10)$$

where,

$$k = k_1 + k_2 + k_3 + k_4 + k_5 \quad (4.11)$$

$$l = l_1 + l_2 + l_3 + l_4 + l_5. \quad (4.12)$$

Each individual probability in equation (4.10) is obtained by using the multinomial statistics [50].

Correspondingly, the  $k$ -fold capture and  $l$ -fold ionization cross section is:

$$\sigma_{kl}^{\alpha\beta\gamma} = \int P_{kl}(\vec{b}, \alpha\beta\gamma) d\vec{b} \quad (4.13)$$

$$= \sum_{k_1, \dots, k_5} \sum_{l_1, \dots, l_5} \int P_{k_1 l_1}^C(\vec{b}_1) P_{k_2 l_2}^{H_1}(\vec{b}_2) P_{k_3 l_3}^{H_2}(\vec{b}_3) P_{k_4 l_4}^{H_3}(\vec{b}_4) P_{k_5 l_5}^{H_4}(\vec{b}_5) d\vec{b}. \quad (4.14)$$

Equation (4.14) cannot be separated into the contributions from each individual atom. Thus, unlike net cross sections, charge-state correlated cross sections depend on molecular orientation. An advantage of the IAM over our molecular method is that within this framework we are not restricted to a specific symmetry. One can consider any arbitrary molecular orientation, whereas in the molecular method only orientations that respect a certain symmetry can be considered (c.f. chapter (3)). Therefore, to study the charge-state correlated events the IAM provides a more flexible framework. Furthermore, the IAM can be applied to any molecular system while our molecular method relies on the compact geometry of the CH<sub>4</sub> molecule.

In this work, however, we have only considered net electron removal cross sections. We have also used the IAM to further investigate the validity of restricting our study to the four orientations that we have considered. This will be explained in the subsequent sections.

## 4.2 Independent Atom Model: Procedure

In the last chapter, it was shown (figures (3.1) and (3.2)) that the four orientations considered in the molecular method were sufficient to yield orientation-averaged cross sections. The IAM can also be used to confirm this.

In the IAM there are five independent ion-atom collisions to be considered: one proton-C collision as well as four proton-H collisions. For net cross sections the IAM

is reduced to Bragg's additivity rule. To perform Bragg's calculations we define a set of impact parameters with respect to the molecular centre, use those impact parameters for all of the atoms and use equations (4.7 and 4.8) to obtain the net cross sections. However, our goal is to study the orientation-dependent probabilities. We average the probabilities of the four molecular orientations:

$$P_{avg}(b) = \frac{1}{4}(P(\vec{b}, \alpha_1\beta_1\gamma_1) + \dots + P(\vec{b}, \alpha_4\beta_4\gamma_4)) \quad (4.15)$$

and if the system is independent of molecular orientation then:

$$\sigma_{avg} = 2\pi \int_0^\infty b P_{avg}(b) db. \quad (4.16)$$

It would be sufficient to consider the four molecular orientations if the following holds:

$$\sigma_{avg} \simeq \sigma_{Bragg} \quad (4.17)$$

since it states that the average cross section of these orientations is approximately the same as the orientation-independent total net cross section and hence, considering more orientations would be unnecessary.

To perform IAM calculations one needs to specify a set of impact parameters with respect to the molecular centre and then find the effective impact parameters for each hydrogen atom. As shown in equation (4.3) the effective atomic impact parameters depend directly on the impact parameter with respect to the carbon atom as well as the Euler angles. Hence, the first task is to find the effective impact parameters.

As an example we consider one of the molecular orientations :  $\alpha = 45, \beta = 90$  and  $\gamma = 180$ .

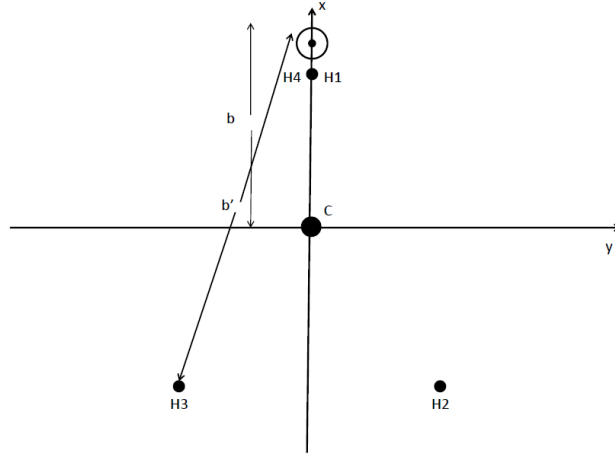


Figure 4.1: The molecular orientation for  $\alpha = 45, \beta = 90$  and  $\gamma = 180$  with respect to the original orientation of [34]. Shown is the projection in the azimuthal plane (x-y).

The coordinate system which corresponds to this orientation can be seen in the top right figure in appendix (D). The projectile is in the x-z plane and moves along the z direction.  $H_1$  and  $H_4$  are in the x-z plane while  $H_2$  and  $H_3$  are mirror images with respect to this plane i.e. they are located in the x-y plane. By projecting the molecule on the azimuthal plane (Figure (4.1)) one can infer the effective individual impact parameters as explained below:

To represent the effective atomic impact parameters, each atom is identified by a subscript (i.e.  $b_{H_i}$  where  $i = 1..4$ ). It is evident from figure (4.1) that the effective impact parameters for  $H_1$  and  $H_4$  are identical. The same also holds for  $H_2$  and  $H_3$ . In each case, in order to determine the effective atomic impact parameters, we first have to find the hydrogen atom positions with respect to the centre,  $\vec{r}_{H_i}$ . The method to do so and the obtained position vectors are shown in appendix (E.1). The effective impact parameters for  $H_1$  and  $H_4$  are obtained by subtracting the

$x$ -component of  $\vec{r}_{H_1}$  (or  $\vec{r}_{H_4}$ ) from  $b$ . Hence:

$$b_{H_1} = b_{H_4} = \left| b - \frac{d}{\sqrt{3}} \right| \quad (4.18)$$

and similarly for  $H_2$  and  $H_3$ :

$$b_{H_2} = b_{H_3} = b' = \sqrt{\left(b + \frac{d}{\sqrt{3}}\right)^2 + \left(\sqrt{\frac{2}{3}}d\right)^2}. \quad (4.19)$$

In a similar manner, the effective impact parameters corresponding to the other orientations are obtained and the results are shown in appendix (E.2).

Thus, the method for a given orientation is as follows: We choose a set of impact parameters with respect to the carbon atom. The effective impact parameter with respect to each one of the hydrogen atoms is then found as explained above. The probabilities at each impact parameter are then calculated and the ones that correspond to each other are added. For example, for the above orientation, when  $b = 0.2$ ,  $b_{H_1} = b_{H_4} = 0.984$  and  $b_{H_2} = b_{H_3} = 2.171$ . The individual capture or ionization probabilities at those impact parameters are then added and weighted by the carbon atom impact parameter,  $b$ . This procedure is done for the entire set of impact parameters to obtain the molecular orientation-dependent probabilities.

Furthermore, for proton-C collision, our basis set includes the carbon  $KLMN$  shell states for the target, hydrogen-like  $KLMN$  shell states for the projectile as well as pseudostates to represent the continuum. For p-H collisions the basis includes hydrogen-like  $KLMN$  shell states on the projectile and the target in addition to the pseudostates.

Figures (4.2) and (4.3) show the net ionization and capture probabilities as functions of impact parameter for  $E = 20, 50$  and  $500$  keV. Although some differences are

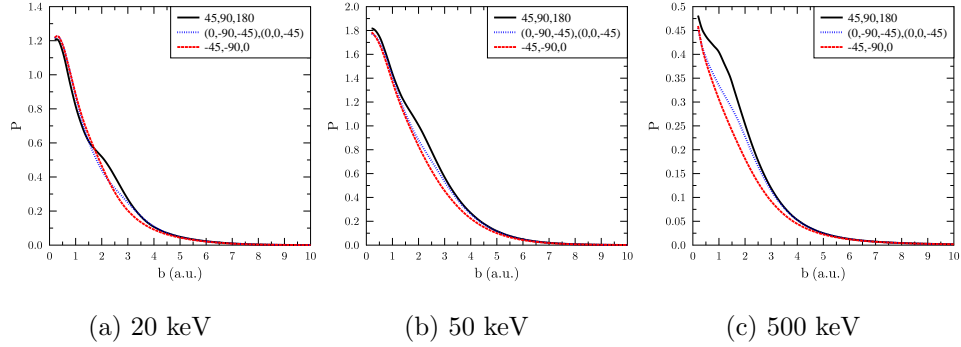


Figure 4.2: Net ionization probability for p-CH<sub>4</sub> collisions calculated within the IAM as a function of impact parameters at impact energies: 20 keV, 50 keV and 500 keV. The considered orientations are:  $(\alpha, \beta, \gamma) = (0, -45, -90), (0, 0, -45), (45, 90, 180)$  and  $(-45, -90, 0)$

observed at low impact parameters, in particular for capture at 50 keV, at larger impact parameters the system becomes almost perfectly orientation independent. Thus, the overall structures imply that approximation (4.17) is fairly accurate.

Figures (4.4) and (4.5) compare the averages of the four molecular orientations with the results obtained by Bragg's additivity rule for capture and ionization respectively. There is practically a perfect agreement between the orientation-averaged cross sections and Bragg's cross sections which indicates that approximations (4.15) and (4.16) are valid and fairly accurate to yield properly averaged cross sections.

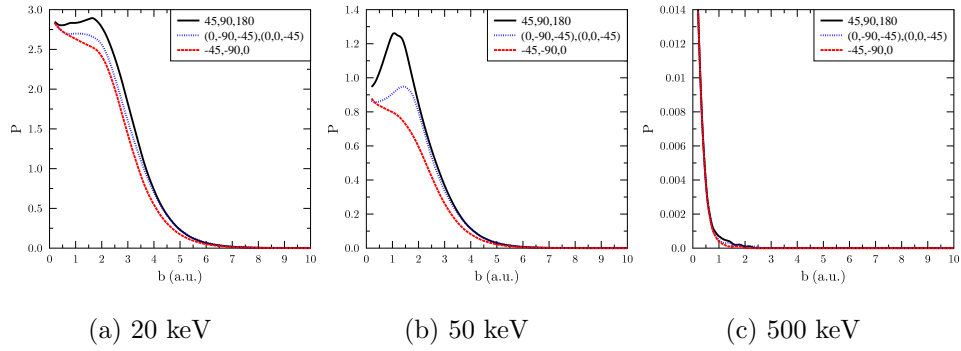


Figure 4.3: Net capture probability for  $p\text{-CH}_4$  collisions calculated within the IAM as a function of impact parameters at impact energies: 20 keV, 50 keV and 500 keV. The considered orientations are:  $(\alpha, \beta, \gamma) = (0, -45, -90), (0, 0, -45), (45, 90, 180)$  and  $(-45, -90, 0)$

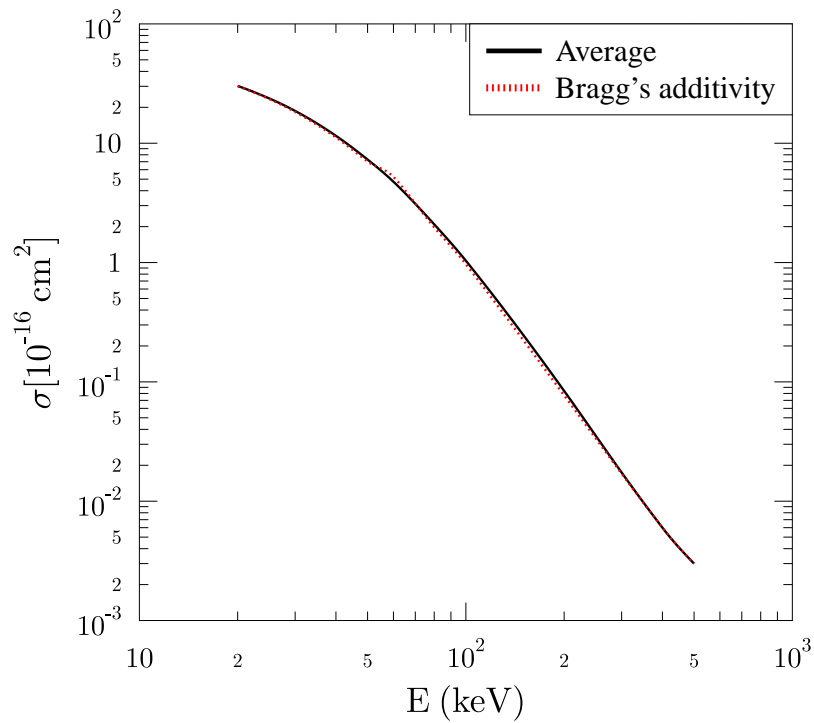


Figure 4.4: Comparison between the average of the capture cross sections of all four orientations and the cross sections obtained by Bragg's additivity rule

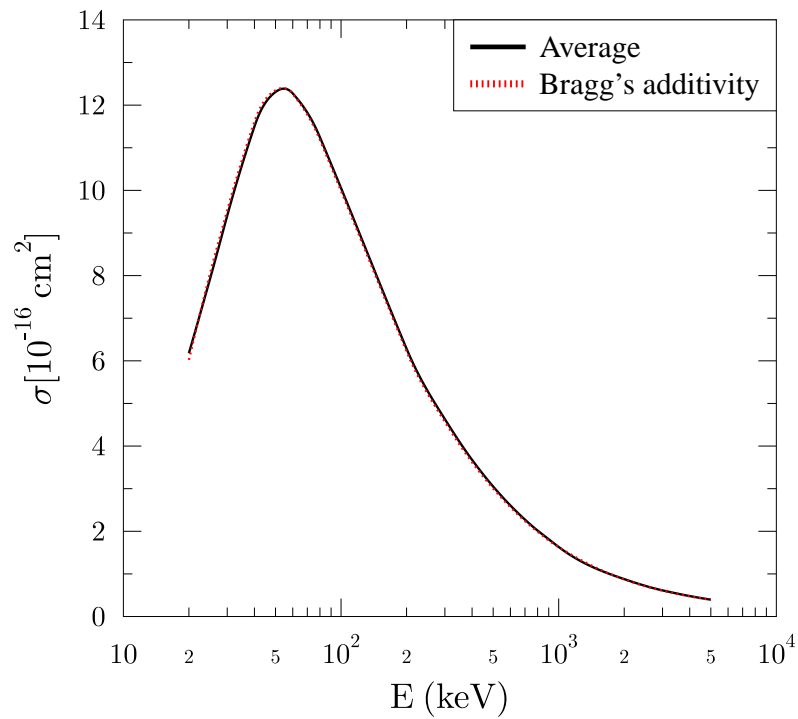


Figure 4.5: Comparison between the average of the ionization cross sections of all four orientations and the cross sections obtained by Bragg's additivity rule

# Chapter 5

## Results

We have used the molecular model (chapter (3)) and Bragg's additivity rule (chapter (4)) to calculate the net ionization and capture cross sections. As mentioned previously, the obtained cross sections are orientation-averaged and hence, can be compared with cross sections from experimental studies. The results are discussed in the subsequent sections.

### 5.1 Ionization

#### 5.1.1 Molecular TC-BGM

Figure (5.1) shows the net ionization cross section (averaged over four orientations) as a function of the impact energy. The same figure on a logarithmic scale (figure (5.2)) is provided to show more detail of the behaviour of the system at large energies. The cross sections are compared with the recommended experimental data from [15].

The solid line shows the net cross sections where excitation is neglected (c.f. equation (3.26)) whereas the dashed line shows the cross sections that take excitation

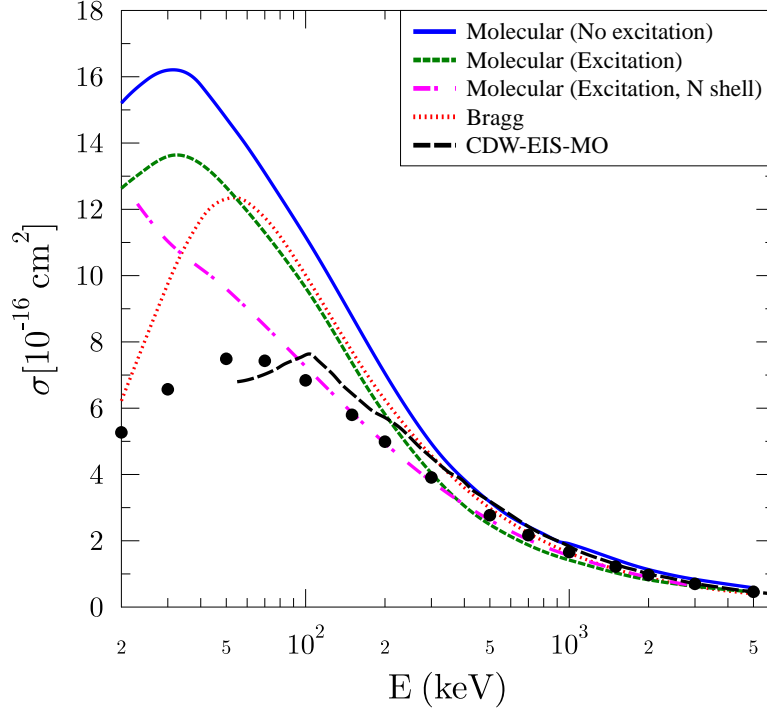


Figure 5.1: Net ionization cross section as a function of impact energy for p-CH<sub>4</sub> collisions. The solid line shows the results obtained from analysis (3.26) The dashed line shows the results obtained from using equation (3.27). For the cross sections shown by the dash-dotted line equation (3.27) has been used and target states of the  $N$  shell are also included in the TC-BGM basis. The dotted line shows the cross section obtained by Bragg's additivity rule. The long dashed lines are the CDW-EIS cross sections from [21]. The experimental data ( $\bullet$ ) are the recommended cross sections from [15] where the experimental data from [6, 11, 12, 13] with their corresponding uncertainties have been combined.

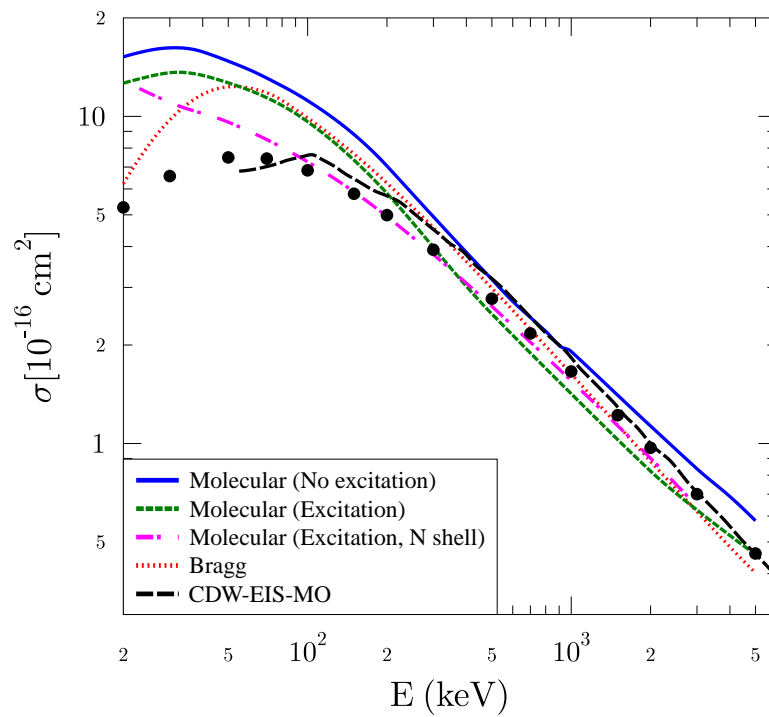


Figure 5.2: Same as figure (5.1) except that the cross section is shown on a logarithmic scale.

into account (equation (3.27)). For these calculations, our basis includes the target states of  $KLM$  shells. Both sets of cross sections agree fairly well at high impact energies as evident from figure (5.2). When excitation is neglected the ionization cross sections are above the experimental data points at all energies. However, when excitation is considered, at high energies, the cross sections are below the experimental data points and cross these at  $E < 300$  keV. For  $E < 300$  keV the situation is similar to the analysis without excitation i.e., ionization is clearly over-estimated particularly at low energies. The position of the peak is also in disagreement with the experimental results. According to the molecular model the maximum cross section occurs at  $E \simeq 30$  keV while the experiment shows a maximum at  $E \simeq 50$  keV. It is interesting that when excitation is considered the results are somewhat improved and the cross sections at lower energies are reduced.

We have further investigated the excitation contribution by including more atomic target states in the basis. We include the  $N$  shell atomic target states in the TC-BGM basis, but we don't use these to represent the initially populated MOs. Therefore, they make no contribution to the molecular ground state, but at the final time it is possible for the electrons to be bound to those states. Furthermore, the set of TC-BGM pseudostates changes since the regularized potential is applied to more target states (c.f. chapter (3)). This analysis allows more room for excitation. One can see that the results improve considerably at large and intermediate energies. However, at  $E < 100$  keV the cross sections start deviating from the experimental ones. The curve does not show a maximum and the cross section continues to increase as we move to lower energies.

One common feature for all these models is the poor behaviour at low impact energies. One reason could be the lack of convergence of the TC-BGM basis set at

low energies. Another reason may be the approximation involved in the spectral representation of the molecular Hamiltonian (equation (3.6)). We have included only five MOs (that represent the molecular ground state) in the sum which can be insufficient particularly at low impact energies. Some numerical issues may also contribute to this problem at low energies particularly for a larger basis set. However, figures (5.1) and (5.2) provide a strong indication of the significance of the excitation channel.

Also shown in figures (5.1) and (5.2) are the results obtained by Bragg's rule and also the results from the CDW-EIS approach. They will be addressed in the subsequent sections.

### 5.1.2 Bragg's rule

The net ionization cross section was also calculated by using Bragg's additivity rule. The corresponding net results as a function of impact energy are shown in figure (5.3) by the dotted curve. While the agreement with the experimental results is good at high energies, at  $E \leq 200$  keV the cross sections are over-estimated. Also shown are the individual components of CH<sub>4</sub>. The hydrogen cross sections are weighted by four to show the contributions of all of the hydrogen atoms. In the low to intermediate energy range ionization is dominated by the hydrogen atoms. At energies above 1 MeV, however, the carbon and the hydrogen cross sections merge and give similar contributions.

To investigate Bragg' additivity rule more thoroughly, we have tested it for the simpler p-H<sub>2</sub> collision system as shown in figure (5.4). We also show the p-H cross section in figure (5.5). For H<sub>2</sub>, a similar trend as for CH<sub>4</sub> can be observed, i.e., at intermediate energies the cross section is well above the experimental data from [6].

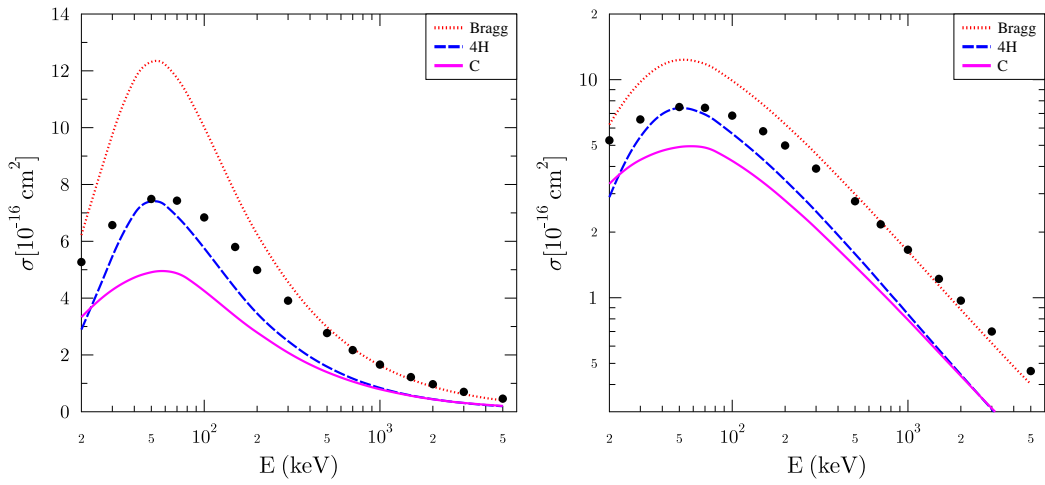


Figure 5.3: Net ionization cross section as a function of impact energy. Shown on the left: semi-logarithmic and on the right: logarithmic scales. The cross sections are obtained by Bragg's additivity rule. Also shown are the individual components i.e., the contributions from the four hydrogen atoms (the dashed line) as well as the contribution from the carbon atom (the solid line). The experimental data ( $\bullet$ ) are the recommended cross sections from [15] where the experimental data from [6, 10, 11, 12, 13, 14] with their corresponding uncertainties have been combined.

The impact energy where the maximum occurs agrees well with the experimental results while the maximum cross section value exceeds the one from the experimental study. This is consistent with what we observe for CH<sub>4</sub>. Similarly, for p-H collision, ionization at intermediate and lower energies is overestimated when compared to the results from [51]. However, it shows a better agreement with the older results from [52]. As evident from all these three cases (p-H, p-H<sub>2</sub> and p-CH<sub>4</sub> collisions) as the number of the hydrogen atoms increases the deviation becomes larger. Thus, figures (5.3, 5.4 and 5.5) suggest that the CH<sub>4</sub> cross sections are overestimated mainly because of the contributions from the hydrogen atoms.

### 5.1.3 Comparisons

Also shown in figures (5.1) and (5.2), by the long dashed lines, are the cross sections obtained in [21] by using the CDW-EIS method. CDW-EIS is a first order distorted wave approximation which is intended to describe ionization at intermediate and high impact energies. In this model, the initial and final states are distorted by being multiplied by a factor [53]. The target bound wavefunction are multiplied by an Eikonal phase factor which accounts for the presence of the projectile field. For ionization, the target continuum wavefunction is multiplied by a Coulomb factor which considers the active electron to be in the projectile continuum simultaneously. These distorted waves satisfy the asymptotic conditions of the Coulomb potential. CDW-EIS has proven to be successful for ion-atom collisions at intermediate and high impact energies [54]. In [21] an extension of this method to molecular targets has been discussed. Similar to our molecular model, the MOs are expanded in single-centred orbitals. The calculations are done in the IEM framework where the single particle equations are solved by the CDW-EIS method. Furthermore, an effective

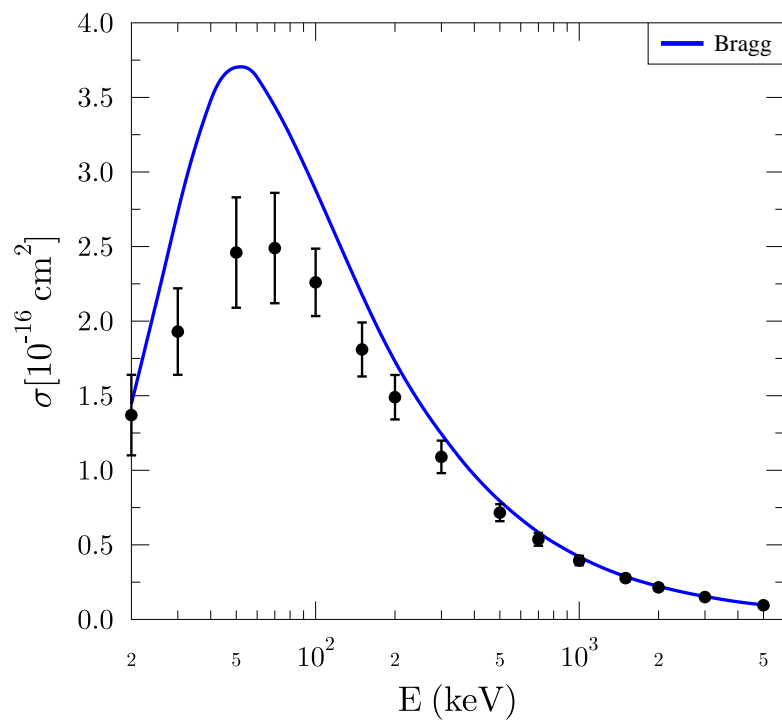


Figure 5.4: Net ionization cross section as a function of impact energy for p-H<sub>2</sub> collisions. The theoretical results (solid line) are obtained by Bragg's additivity rule. The experimental data (●) are from [6]

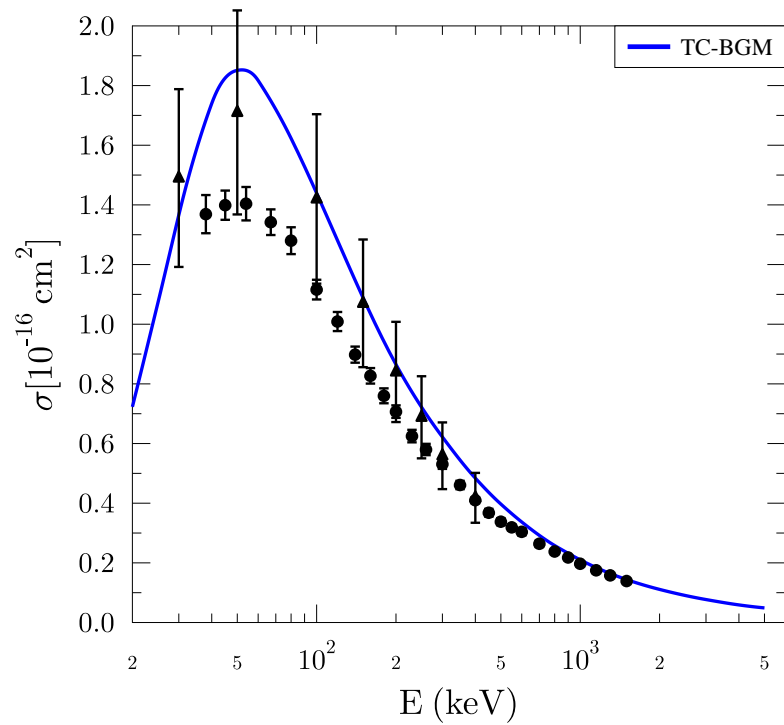


Figure 5.5: Ionization cross section as a function of impact energy for p-H collisions. The experimental data (●) are from [51] and (▲) are from [52]

bond length has been used which is the product of the equilibrium bond length and a parameter,  $a$ . The equilibrium distance that is used in that study is 2.106 a.u. (as opposed to 2.05 in our study) with the parameters being  $a = 1.0$  and  $a = 0.7$ . It has been shown in the paper that  $a = 0.7$  yields better agreement with the experimental results.

At high impact energies all models show good agreement with the experimental results particularly the CDW-EIS calculations as well as our molecular model when excitation is considered and the target  $N$  shell is included. At intermediate energies, however, the situation is less clear and the models behave differently. The experimental results for  $100 \leq E \leq 5000$  keV are best predicted by the molecular method with a larger basis when excitation is considered. CDW-EIS also agrees fairly well with the experimental data points for this energy range although the cross sections are slightly above the experimental points. However, at  $E \leq 100$  keV it behaves poorly which shows the limitations of this model at lower energies.

Furthermore, in Bragg's rule all of the atoms are equally weighted. This is not the case in the molecular method since the AOs are centred on the carbon atom and hence, the contribution from the hydrogen atoms might be underestimated. The differences between these treatments can lead to the observed disagreement between the two models at lower energies.

## 5.2 Capture

### 5.2.1 Molecular TC-BGM

We have considered capture for energies up to 200 keV. For higher impact energies capture is so small that numerically, the TC-BGM calculations become unreliable.

Figures (5.6) and (5.7) show the net capture cross section that was obtained by the molecular TC-BGM calculations. We have included the target *KLM* shell states in the basis. The calculations with a larger basis as for ionization was unnecessary since the capture cross section is practically unaffected by the change in basis. Hence, we used a smaller basis set as they make calculations less challenging numerically. Also shown are the experimental results from [6, 16, 52]. Overall, the agreement is satisfactory, although the experimental data are somewhat overestimated by our calculations. At  $E \geq 100$  keV the situation is better and the calculated cross sections are consistent with the experimental data.

### 5.2.2 Bragg's rule

Figure (5.8) shows the net capture cross section obtained by Bragg's rule as a function of the impact energy. Also shown are the contributions from the individual atoms. The experimental results are well predicted by Bragg's additivity rule at energies higher than 50 keV. However, at  $E \leq 50$  keV the model clearly overestimates capture. Similar to ionization, the four hydrogen atoms dominate the cross section at low energies and as can be seen from the figure, the calculated 4H cross sections, alone, have higher values than the measured CH<sub>4</sub> cross sections. This can also be seen from the analysis of H<sub>2</sub> as shown in figure (5.9). The calculated net capture cross section for H<sub>2</sub> is considerably higher than the experimental data points at low energies. The reason is that e.g. for CH<sub>4</sub> according to Bragg's rule, we have to consider four p-H collisions in which electron capture becomes resonant toward low impact energies whereas there is no such resonance for p-CH<sub>4</sub>. However, Bragg's additivity rule fails to take that into account. Therefore, in order to use Bragg's additivity rule in this energy regime one has to make corrections. One suggested

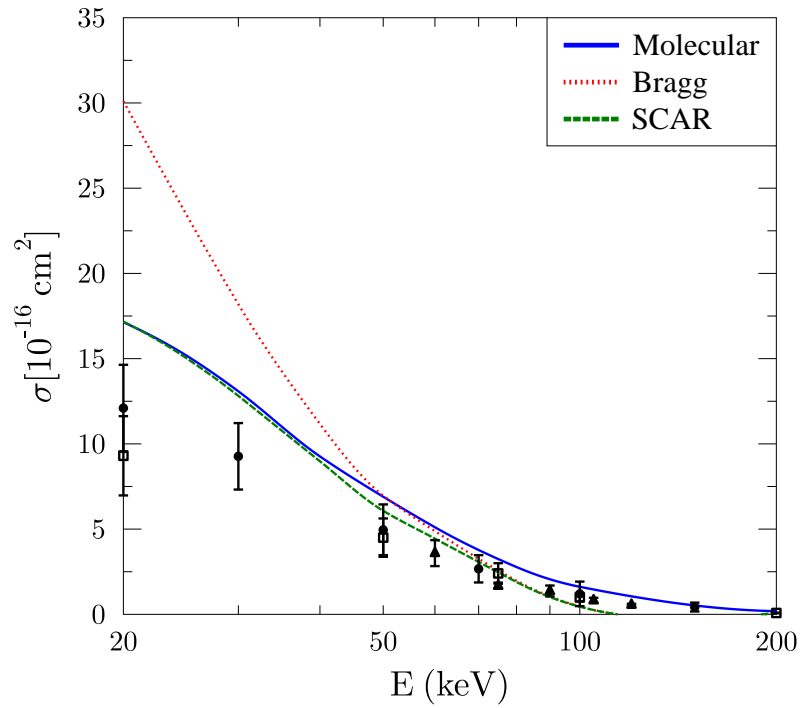


Figure 5.6: Net capture cross section as a function of impact energy for p-CH<sub>4</sub> collisions. The solid line shows the cross section obtained from the molecular TC-BGM. The dotted curve shows the cross section obtained from Bragg’s additivity rule. The dashed curve represents the SCAR result. The experimental data shown by (•), (□) and (▲) are from [6], [52] and [16], respectively.

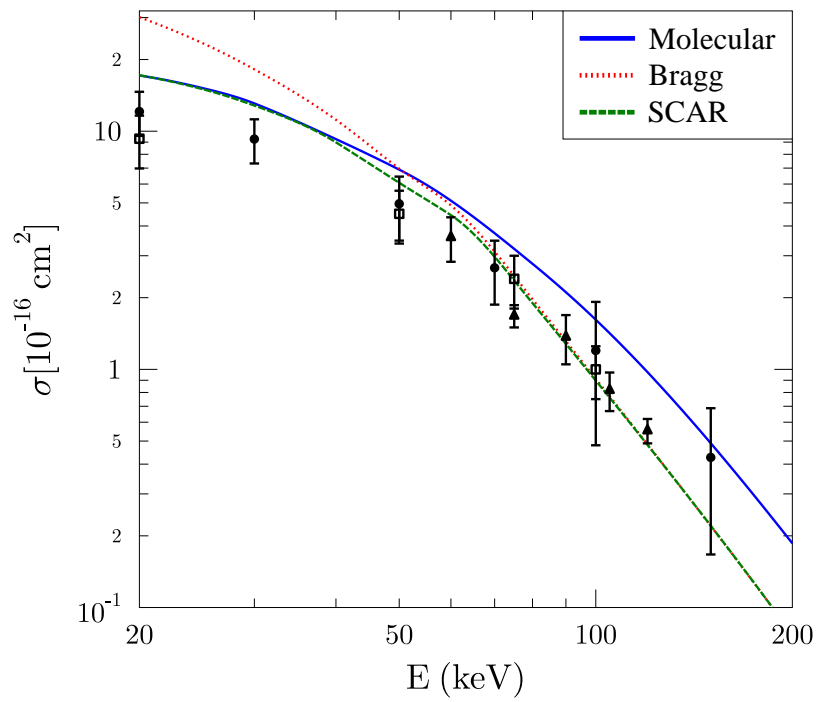


Figure 5.7: Same as figure (5.6) except that the cross section is shown on a logarithmic scale.

model to correct Bragg's additivity is the screening corrected additivity rule, SCAR [55]. It has been argued in [55] that at low energies individual atoms cannot be considered as independent scatterers and there are multiple scatterings within a molecule. To that end, a screening coefficient has been introduced and multiplied to each atomic cross section to account for the overlaps between the atoms.

$$\sigma^{SCAR} = \sum_i s_i \sigma_i \quad (5.1)$$

with  $0 \leq s_i \leq 1$ . This model was originally suggested for electron-molecule scattering. However, we use it for the electron capture channel for this collision system (i.e., an ion-impact collision) although its applicability is not obvious. It is interesting to see (figures(5.6) and (5.7)) that the results obtained with using the screening coefficients given in [55] are significantly improved compared to the standard Bragg results.

At energies higher than 50 keV Bragg's additivity rule predicts the experimental results better than the molecular model while at low energies the molecular model is more consistent with the experiments. However, the best results are obtained when the SCAR treatment is applied to Bragg's rule.

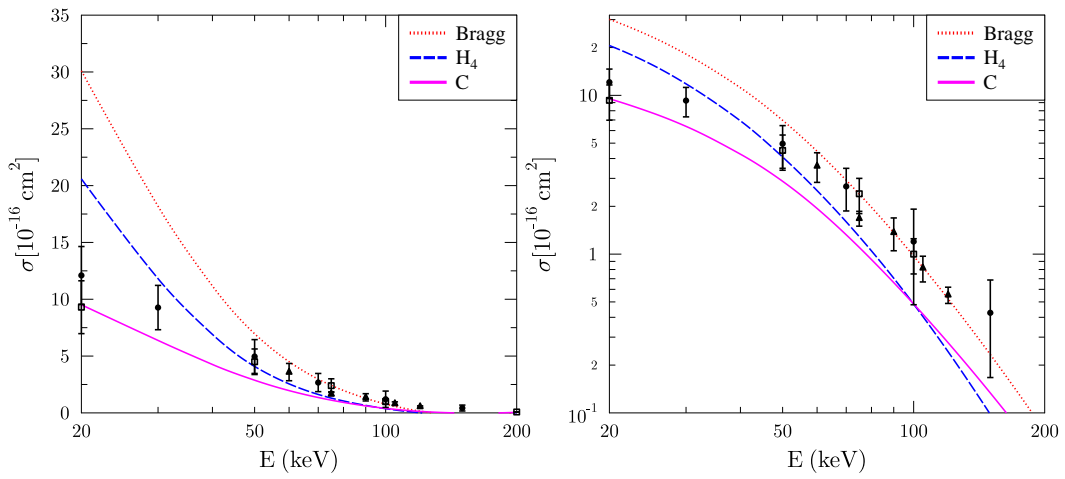


Figure 5.8: Net capture cross section as a function of impact energy for p-CH<sub>4</sub> collisions. The cross section is obtained by Bragg's additivity rule. Also shown are the individual components i.e. the contributions from the hydrogen atoms (the dashed line) as well as the contribution from the carbon atom (the solid line). The experimental data shown by (●), (□) and (▲) are from [6], [52] and [16] respectively.

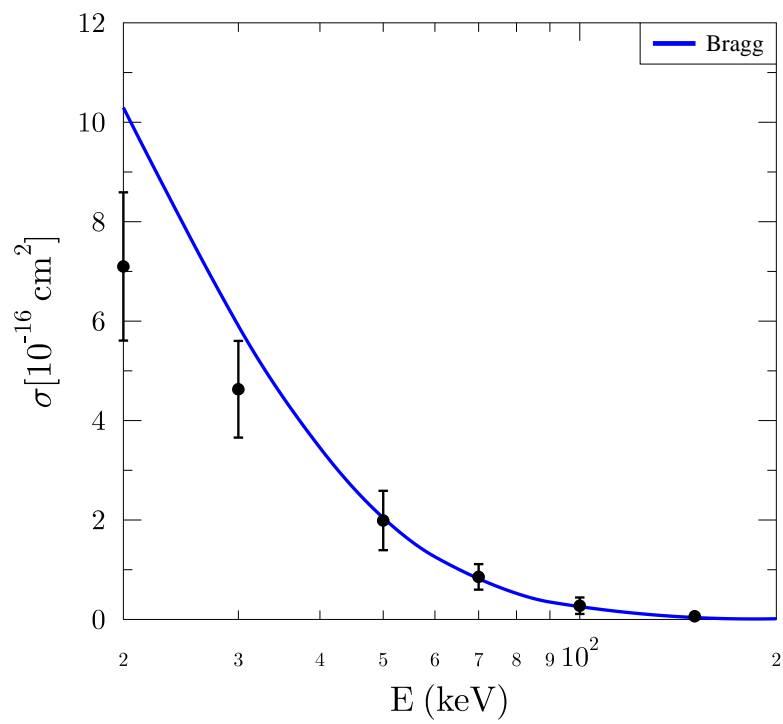


Figure 5.9: Net capture cross section as function of impact energy for  $p\text{-H}_2$  collisions. The cross sections are obtained by Bragg's additivity rule. The experimental data shown by ( $\bullet$ ) are from [6].

## Chapter 6

# Conclusions

We have presented a quantum mechanical analysis of the electron removal processes in proton-methane collisions in an impact energy range from 20 keV to 5 MeV. The projectile is assumed to move on a classical straight-line trajectory. The independent electron model was used to approximate the full many-electron time-dependent Schrödinger equation and the single-electron Schrödinger equations were solved by the two-centre basis generator method.

We investigated the electron removal processes by means of calculating the net ionization and capture cross sections. Two methods were used to study the collision system. One was the molecular TC-BGM model and the second model was the independent atom model in which we performed five individual ion-atom collision calculations by using the TC-BGM.

The molecular approach is based on two ideas: Using the spectral representation for the target Hamiltonian and an expansion of the MOs into an orthogonal, single centred basis set. The MOs were expanded into orbitals that are centred on the carbon atom. This approximation was based on the compact geometry of the

methane molecule.

For the net capture probability we considered the electrons that populate the projectile's bound states at the final time. For net ionization the electrons that were neither in the molecular ground state MOs nor in the projectile's bound states at the final time were considered to be ionized. Alternatively, we considered the electrons to be bound to the target as long as they were in any of the atomic target states (not necessarily contributing to the molecular ground state). This allowed us to estimate the excitation processes.

A drawback of this model is that we were restricted to four molecular orientations only. To obtain the orientation-averaged cross section we showed that to a good approximation the system is independent of the molecular orientation and therefore, the four orientations were sufficient to yield properly averaged cross sections. The cross sections were calculated by averaging the net probabilities for the four orientations.

The insensitivity of the collision system to the molecular orientation was further tested and verified by using the independent atom model to study the orientation-dependent probabilities. We showed that the orientation-averaged cross sections were approximately the same as Bragg's cross sections, i.e., considering the average probabilities to be orientation-independent was a valid approximation. Finally, we used Bragg's additivity rule to obtain the net ionization and capture cross sections.

For ionization both models predict the experimental results fairly well. At intermediate energies, however, Bragg's additivity rule overestimates ionization. Similarly, the molecular TC-BGM model predicts even higher net ionization cross sections when no excitation is considered. However, when excitation is considered, the results are improved. To allow more room for excitation, we added the  $N$  shell

target atomic states to the TC-BGM basis. Using this analysis, we obtain an almost perfect agreement for the energy range of  $100 \leq E \leq 5000$  keV. However, the behaviour at low energies is unphysical since no maximum occurs. Despite the issues at low energies, these results strongly indicate the importance of excitation processes in this collision system and when considered, the results for ionization are significantly improved.

We also compared our results to the perturbative continuum distorted wave-eikonal initial state calculations in [21]. Similar to other models, the CDW-EIS calculations predict the experimental ionization cross section well at high energies and the overall agreement is good for energies higher than 100 keV, but the method has limitations at lower energies.

For capture the situation is similar to ionization at high energies i.e., both the molecular model and Bragg's rule are fairly consistent with the experimental data. Bragg's calculations show a very good agreement at high energies but at intermediate and low energies the cross section is highly overestimated. The molecular model, however, predicts the overall behaviour of the cross section although the values are overestimated. A significant improvement to Bragg's calculations at low energies is achieved by using the screening corrected additivity rule. A more detailed study of the SCAR treatment will be the subject of future studies.

In conclusion, the molecular model agrees well with experimental results for both ionization and capture except at low energies. Although in principle this method was exact within the independent electron model, a number of approximations were made. In the spectral representation of the Hamiltonian for instance, we only used the bound target states that contribute to the molecular ground state while in principle an infinite number of states (both bound and unbound states) have to

be considered. Also the TC-BGM basis was not a complete basis in practice and increasing the basis size imposes major numerical difficulties. Furthermore, we approximated excitation in a crude way since there exist no molecular excited states in our analysis. Overall, it can be argued that the results are good at energies of around 100 keV and higher particularly for ionization when excitation is considered. Similarly, Bragg's rule is applicable particularly at high energies. However, both of these models have limitations at low energies.

The goal of this project was to calculate the net ionization and capture cross sections. However, in the longer run, the study of fragmentation processes is of interest. For fragmentation processes one has to deal with more detailed cross sections i.e. charge-state correlated cross sections. However, the independent atom model can be used since it deals with the orientation dependent probabilities. An advantage of this model is that it is not restricted to any specific molecular orientation which makes it a more flexible model to study the charge-state correlated states. As a result, it can be extended to study other hydrocarbons in the future.

# Appendix A

## Spherical Harmonics

The complex spherical harmonics are given by [56]:

$$Y_l^m(\theta, \phi) = \sqrt{\frac{2l+1}{4\pi} \frac{(l-m)!}{(l+m)!}} P_l^m(\cos\theta) e^{im\phi} \quad (\text{A.1})$$

$$Y_l^{-m} = (-1)^m (Y_l^m)^* \quad (\text{A.2})$$

$$Y_l^0 = \sqrt{\frac{2l+1}{4\pi}} P_l(\cos\theta) \quad (\text{A.3})$$

where  $P_l(x)$  is the Legendre polynomial of order  $l$  and the  $P_l^m(x)$  are the associated Legendre functions. The first few normalized spherical harmonics with the corresponding associated Legendre functions are shown in [56]. The carbon  $2p$  STOs can be written in terms of the complex spherical harmonics in the following way:

$$2p_0 = \chi_{2,1,0}(r, \theta, \phi) = N r e^{-Zr} Y_1^0 \quad (\text{A.4})$$

$$2p_1 = \chi_{2,1,1}(r, \theta, \phi) = N r e^{-Zr} Y_1^1 \quad (\text{A.5})$$

$$2p_{-1} = \chi_{2,1,-1}(r, \theta, \phi) = N r e^{-Zr} Y_1^{-1} \quad (\text{A.6})$$

where  $N$  is the normalization constant.

Alternatively, the  $2p$  orbitals can be stated in terms of the real spherical harmonics. The real spherical harmonics are explained in detail in [57]. For  $m = 0$ :

$$Y'_{l,0} = Y_l^0 \quad (\text{A.7})$$

However, for  $m \neq 0$  we define the gerade, g, and ungerade, u, orbitals as the following:

$$Y'_{l,m_g} = \sqrt{\frac{2l+1}{2\pi} \frac{(l-m)!}{(l+m)!}} P_l^m(\cos\theta) \cos(m\phi) \quad (\text{A.8})$$

$$Y'_{l,m_u} = \sqrt{\frac{2l+1}{2\pi} \frac{(l-m)!}{(l+m)!}} P_l^{-m}(\cos\theta) \sin(-m\phi) \quad (\text{A.9})$$

The real spherical harmonics with  $m \neq 0$  can also be written in terms of the complex spherical harmonics:

$$Y'(\theta, \phi)_{l,m_g} = \frac{1}{\sqrt{2}} [Y_l^m(\theta, \phi) + (-1)^m Y_l^{-m}(\theta, \phi)] \quad (\text{A.10})$$

$$Y'(\theta, \phi)_{l,m_u} = \frac{i}{\sqrt{2}} [(-1)^m Y_l^m(\theta, \phi) - Y_l^{-m}(\theta, \phi)] \quad (\text{A.11})$$

Consequently, the  $2p$  orbitals, in terms of the real spherical harmonics, obtain the following form:

$$2p_z = \chi_{210}(r, \theta, \phi) = N r e^{-Zr} Y'_{1,0} \quad (\text{A.12})$$

$$2p_x = \chi_{211_g}(r, \theta, \phi) = N r e^{-Zr} Y'_{1,1_g} \quad (\text{A.13})$$

$$2p_y = \chi_{211_u}(r, \theta, \phi) = N r e^{-Zr} Y'_{1,1_u} \quad (\text{A.14})$$

It is important to note that these definitions are not unique. For example, the defi-

nitions of  $2p_x$  and  $2p_y$  can be switched. However, we are using (A.12),(A.13),(A.14) for  $2p_z$ ,  $2p_x$  and  $2p_y$  respectively.

## Appendix B

# Two-centre integrals

In this section we describe a method to calculate integrals of type  $\langle \varphi_{nlm} | S \rangle$  for the cases where the  $|S\rangle$  STOs are centred on the hydrogen atoms. In those cases we have to deal with two-centre integrals. The method is based on rotating the coordinate system such that the hydrogen atom under consideration is on the same axis as the carbon atom. Once the rotation is done we perform the two-centre integral in elliptical coordinates. Here we show the technique to rotate the coordinate system:

$$\langle \varphi_{(g/u),nlm} | H_{1s} \rangle = \langle \varphi_{(g/u),nlm} | H_{100} \rangle \quad (\text{B.1})$$

$$= \langle \varphi_{(g/u),nlm} | \hat{R}^{-1} \hat{R} | H_{100} \rangle \quad (\text{B.2})$$

$$= \langle \tilde{\varphi}_{(g/u),nlm} | \hat{R} | H_{100} \rangle \quad (\text{B.3})$$

$$= \sum_M \langle \tilde{\varphi}_{(g/u),nlm} | \hat{R} | \tilde{\varphi}_{(g/u),nlM} \rangle \langle \tilde{\varphi}_{(g/u),nlM} | H_{100} \rangle \quad (\text{B.4})$$

$$= \langle \tilde{\varphi}_{(g/u),nlm} | \hat{R} | \tilde{\varphi}_{g,nl0} \rangle \langle \tilde{\varphi}_{g,nl0} | H_{100} \rangle \quad (\text{B.5})$$

The  $\langle \tilde{\varphi}_{nlm} | \hat{R} | \tilde{\varphi}_{nlM} \rangle$  can be written in terms of the Wigner matrices [58].

## Appendix C

# Expansion Coefficients

The following table shows an example of the expansion coefficients (c.f. equations 3.16 and 3.18) for  $(\alpha, \beta, \gamma) = (0, -90, -45)$ . It is evident from the table that each MO is strongly dominated by one AO. The  $1a_1$  MO is strongly dominated by carbon  $1s$ .  $2a_1$  is dominated by carbon  $2s$ . The  $1t_{2(x,y,z)}$  MOs are dominated by carbon  $2p_x$ ,  $2p_y$  and  $2p_z$  respectively.

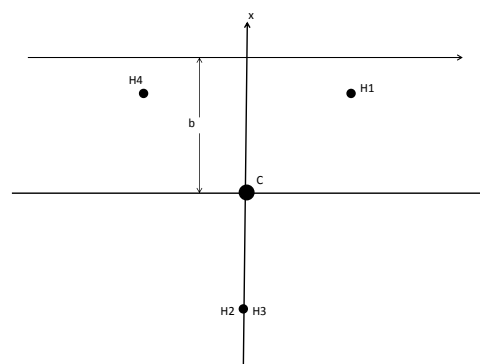
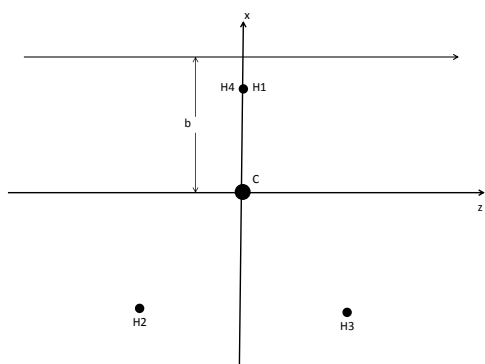
Table C.1: The  $D$  coefficients for each orthonormalized MO. They are obtained after the rotation of the initial coordinate system.

	$1a_1$	$2a_1$	$1t_{2x}$	$1t_{2y}$	$1t_{2z}$
$D_{100g}$	0.99999765	0.00206985	0.00000000	0.00000000	0.00000000
$D_{200g}$	0.00214205	-0.99604329	0.00000000	0.00000000	0.00000000
$D_{210g}$	0.00000000	0.00000000	-0.99546146	0.00000000	0.00000000
$D_{211g}$	0.00000000	0.00000000	0.00000000	0.00000000	-0.99546146
$D_{211u}$	0.00000000	0.00000000	0.00000000	-0.99546146	0.00000000
$D_{300}$	0.00032914	0.08884528	0.00000000	0.00000000	0.00000000
$D_{310g}$	0.00000000	0.00000000	-0.00852965	0.00000000	0.00000000
$D_{311g}$	0.00000000	0.00000000	0.00000000	0.00000000	-0.00852965
$D_{311u}$	0.00000000	0.00000000	0.00000000	-0.00852965	0.00000000
$D_{320g}$	0.00000000	0.00000000	0.00000000	0.00000000	0.00000000
$D_{321g}$	0.00000000	0.00000000	0.00000000	0.00000000	-0.09478250
$D_{321u}$	0.00000000	0.00000000	0.00000000	0.09478250	0.00000000
$D_{322g}$	0.00000000	0.00000000	-0.09478253	0.00000000	0.00000000
$D_{322u}$	0.00000000	0.00000000	0.00000000	0.00000000	0.00000000

## Appendix D

# Molecular Orientations

The four molecular orientations that we considered  $((\alpha, \beta, \gamma) = (0, -90, -45), (0, 0, -45), (45, 90, 180)$  and  $(-45, -90, 0)$ ) are shown below in the collision plane:



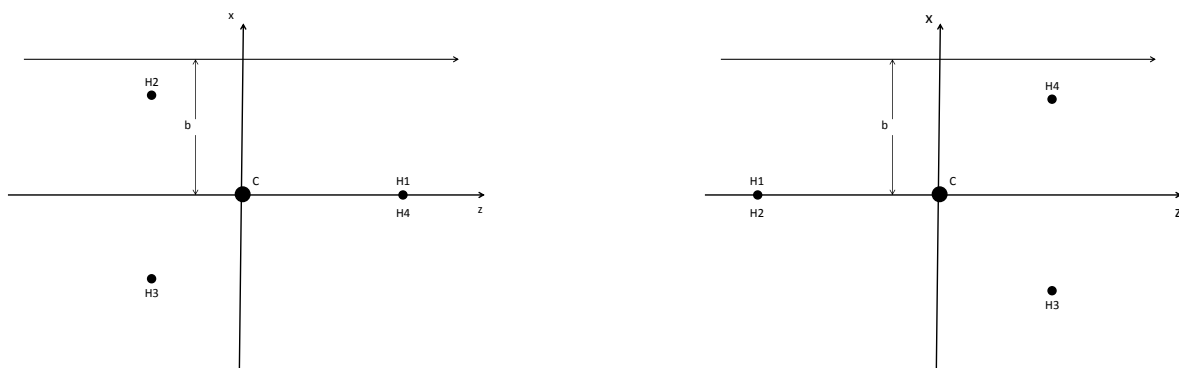


Figure D.2: The four molecular orientations that were considered: Top left)  $(-45, -90, 0)$ , Top right)  $(45, 90, 180)$ , Bottom left)  $(0, 0, -45)$ , Bottom right)  $(0, -90, -45)$

# Appendix E

## Independent Atom Model

### E.1 Calculation of Position Vectors

To obtain the position vectors, we first have to obtain Euler's rotation matrix (using the z-y-z convention):

$$D = D_\gamma D_\beta D_\alpha \tag{E.1}$$

where:

$$D_\gamma = \begin{pmatrix} \cos \gamma & \sin \gamma & 0 \\ -\sin \gamma & \cos \gamma & 0 \\ 0 & 0 & 1 \end{pmatrix} \tag{E.2}$$

$$D_\beta = \begin{pmatrix} \cos \beta & 0 & -\sin \beta \\ 0 & 1 & 0 \\ \sin \beta & 0 & \cos \beta \end{pmatrix} \tag{E.3}$$

$$D_\alpha = \begin{pmatrix} \cos \alpha & \sin \alpha & 0 \\ -\sin \alpha & \cos \alpha & 0 \\ 0 & 0 & 1 \end{pmatrix} \quad (\text{E.4})$$

Thus, for  $\alpha = 45, \beta = 90$  and  $\gamma = 180$ :

$$D = \begin{pmatrix} 0 & 0 & 1 \\ 0.707 & -0.707 & 0 \\ 0.707 & 0.707 & 0 \end{pmatrix} \quad (\text{E.5})$$

The position vectors are then obtained by using  $D$  to rotate the initial coordinate system. The obtained position vectors are:

$$\vec{r}_{H_1} = \frac{d}{\sqrt{3}} \begin{pmatrix} 1 \\ 0 \\ \sqrt{2} \end{pmatrix} \quad (\text{E.6})$$

$$\vec{r}_{H_2} = \frac{d}{\sqrt{3}} \begin{pmatrix} -1 \\ \sqrt{2} \\ 0 \end{pmatrix} \quad (\text{E.7})$$

$$\vec{r}_{H_3} = \frac{d}{\sqrt{3}} \begin{pmatrix} -1 \\ -\sqrt{2} \\ 0 \end{pmatrix} \quad (\text{E.8})$$

$$\vec{r}_{H_4} = \frac{d}{\sqrt{3}} \begin{pmatrix} 1 \\ 0 \\ -\sqrt{2} \end{pmatrix} \quad (\text{E.9})$$

for the internuclear distance,  $d = 2.05$  a.u. (c.f. chapter 2).

## E.2 Effective Impact Parameters

The molecular orientation corresponding to  $(\alpha, \beta, \gamma) = (45, 90, 180)$  is shown and discussed in chapter (4) (c.f. figure (4.1)). The rest of the orientations with the corresponding equations for the effective impact parameters are shown below:

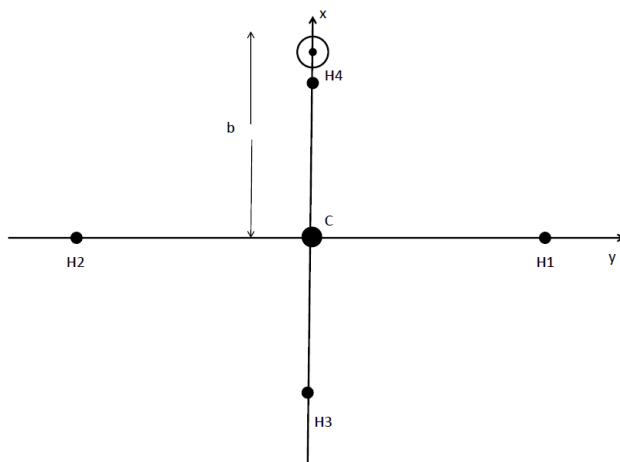


Figure E.1: The molecular orientation for  $\alpha = 0, \beta = -90$  and  $\gamma = -45$  with respect to the original orientation of [34]. Shown is the projection in the azimuthal plane (x-y). The effective hydrogen impact parameters are:

$$\begin{aligned}
 b_{H_1} &= b_{H_2} = \sqrt{b^2 + \frac{2}{3}d^2} \\
 b_{H_3} &= b + \sqrt{\frac{2}{3}}d \\
 b_{H_4} &= |b - \sqrt{\frac{2}{3}}d|
 \end{aligned}$$

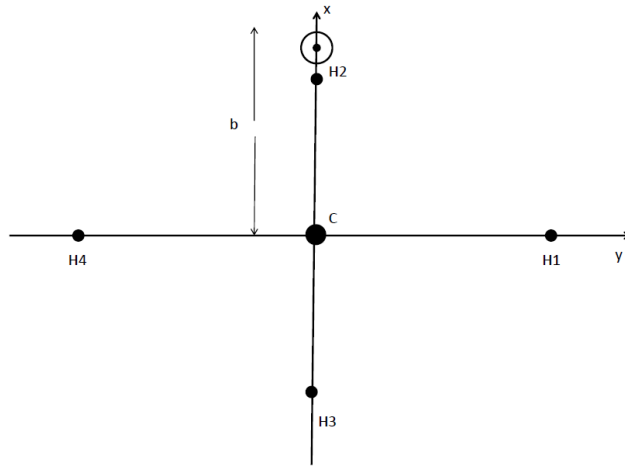


Figure E.2: The molecular orientation for  $\alpha = 0, \beta = 0$  and  $\gamma = -45$  with respect to the original orientation of [34]. Shown is the projection in the azimuthal plane (x-y). The effective hydrogen impact parameters are:

$$b_{H_1} = b_{H_4} = \sqrt{b^2 + \frac{2}{3}d^2}$$

$$b_{H_3} = b + \sqrt{\frac{2}{3}}d$$

$$b_{H_2} = |b - \sqrt{\frac{2}{3}}d|$$

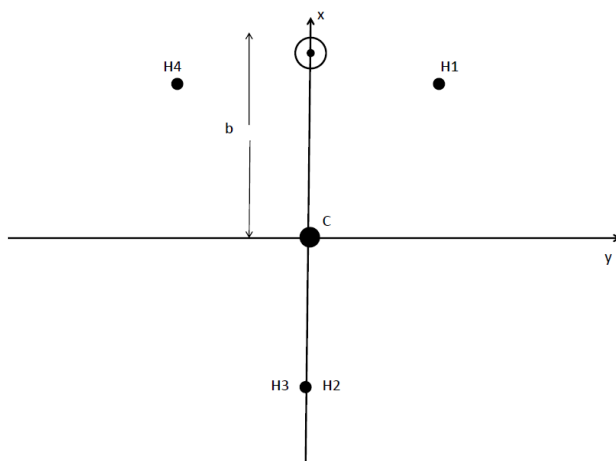


Figure E.3: The molecular orientation for  $\alpha = -45, \beta = -90$  and  $\gamma = 0$  with respect to the original orientation of [34]. Shown is the projection in the azimuthal plane (x-y). The effective hydrogen impact parameters are:

$$b_{H_1} = b_{H_4} = \sqrt{\left(b - \frac{d}{\sqrt{3}}\right)^2 + \frac{2}{3}d^2}$$

$$b_{H_2} = b_{H_3} = b + \frac{d}{\sqrt{3}}$$

# Bibliography

- [1] T.E. Cravens, C.J. Lindgren, and S.A. Levina. *Planet.Space Sci.*, 46:1193, 1998.
- [2] R. Browning and H.B. Gilbody. *J.Phys.B:At.Mol.Phys.*, 1:1149, 1968.
- [3] I. Ben-Itzhak, K.D. Carnes, S.G. Ginther, D.T. Johnson, P.J. Norris, and O.L. Weaver. *Phys.Rev.A*, 47:3748, 1993.
- [4] I. Ben-Itzhak, K.D. Carnes, D.T. Johnson, P.J. Norris, and O.L. Weaver. *Phys.Rev.A*, 49:881, 1994.
- [5] H. Luna, E.G. Cavalcanti, J. Nickles, G.M. Sigaud, and E.C. Montenegro. *J.Phys.B:At.Mol.Opt.Phys.*, 36:4717, 2003.
- [6] M.E. Rudd, R.D. DuBois, L.H. Toburen, C.A. Ratcliffe, and T.V. Goffe. *Phys. Rev. A*, 28:3244, 1983.
- [7] H. Knudsen, U. Mikkelsen, K. Paludan, K. Kiresbom, S.P. Möller, E. Uggerhøj, J. Slevin, M. Charlton, and E. Morenzoni. *J.Phys.B:At.Mol.Opt.Phys.*, 28:3569, 1995.
- [8] T. Cechan and C.R. Vidal. *J.Phys.B:At.Mol.Opt.Phys.*, 31:895, 1998.
- [9] C. Backx and M.J. Van der Wiel. *J.Phys.B:At.Mol.Opt.Phys.*, 8:3020, 1975.

- [10] J. Desesquelles, G.D. Cao, and M.C. Dufay. *C.R. Acad. Sci. Ser. B*, 262:1329, 1966.
- [11] J.G. Collins and P. Kebarle. *J. Chem. Phys.*, 46:1082, 1967.
- [12] R.J. McNeal. *J. Chem. Phys.*, 53:4308, 1970.
- [13] D.J. Lynch, L.H. Toburen, and W.E. Wilson. *J. Chem. Phys.*, 64:2616, 1976.
- [14] R. Mach, H. Drost, H. Behlke, and H.-J. Spangenberg. *Ann. Phys. (Leipzig)*, 34:175, 1977.
- [15] M.E. Rudd, Y.-K. Kim, D.H. Madison, and J.W. Gallagher. *Rev. Mod. Phys.*, 57:965, 1985.
- [16] J.M.Sanders, S.L.Varghese, C.H.Fleming, and G.A.Soosai. *J. Phys. B*, 36:3835, 2003.
- [17] L.H.Toburen, M.Y.Nakai, and R.A.Langley. *Phys. Rev*, 171:114, 1968.
- [18] S.L. Varghese, J.M. Joyce, and R. Laubert. *Phys. Rev. A*, 31:2202, 1985.
- [19] K.H. Berkner, R.V. Pyle, and J.W. Stearns. *Nucl. Fusion*, 10:145, 1970.
- [20] D.W. Koopman. *J. Chem. Phys.*, 49:5203, 1968.
- [21] L. Gulyás, I. Tóth, and L. Nagy. *J.Phys.B:At.Mol.Opt.Phys.*, 46:075201, 2013.
- [22] D.S.F. Crothers and J.F. McCann. *J.Phys.B:At.Mol.Phys.*, 16:3229, 1983.
- [23] I.N. Levine. *Quantum Chemistry*. Prentice-Hall, 5 edition, 2000.
- [24] M. Baer. *Beyond Born-Oppenheimer: electronic nonadiabatic coupling terms and conical intersections*. Wiley, 1 edition, 2006.

- [25] J. Patterson and B. Bailey. *Solid-State Physics: Introduction to the theory*. Springer, 2 edition, 2010.
- [26] M. Baer and R. Englman. *Chem. Phys. Lett.*, 265:105, 1997.
- [27] A.M. Wodtke, J.C. Tully, and D.J. Auerbach. *Int. Rev. Phys. Chem.*, 23:513, 2004.
- [28] R.T. Pack and J.O. Hirschfelder. *J. Chem. Phys.*, 52:521, 1970.
- [29] M. Baer, S.H. Lin, A. Alijah, S. Adhikari, and G.D. Billing. *Phys. Rev. A*, 62:032506, 2000.
- [30] H. Haken and H.C. Wolf. *Molecular Physics and Elements of Quantum Chemistry*. Springer, 2 edition, 2003.
- [31] J.C. Slater. *Phys. Rev. A*, 81:385, 1951.
- [32] D.R. Hartree. *Rep. Prog. Phys.*, 11:113, 1947.
- [33] E. Engel and R.M. Dreizler. *Density Functional Theory: An Advanced Course*. Theoretical and Mathematical Physics. Springer, 2011.
- [34] R.M. Pitzer. *J.Chem.Phys*, 46:4871, 1967.
- [35] W. Meyer. *J.Chem.Phys*, 58:1017, 1973.
- [36] K. Kuchitsu and L.S. Bartell. *J.Chem.Phys*, 36:2470, 1962.
- [37] B.J. Woznick. *J.Chem.Phys*, 40:2860, 1964.
- [38] M. Krauss. *J.Chem.Phys*, 38:564, 1963.
- [39] D.R. Garmer and J.B. Anderson. *J.Chem.Phys*, 86:4025, 1987.

- [40] J.D. Talman and W.F. Shadwick. *Phys. Rev. A*, 14:36, 1976.
- [41] O.J. Kroneisen, H.J. Lüdde, T. Kirchner, and R.M. Dreizler. *J.Phys.A:At.Mol.Opt.Phys.*, 32:2141, 1999.
- [42] M. Zapukhlyak, T. Kirchner, H.J. Lüdde, S. Knoop, R. Morgenstern, and R. Hoeksta. *J.Phys.B:At.Mol.Opt.Phys.*, 38:2353, 2005.
- [43] T. Kusakabe, K. Asahina, A. Iida, Y. Tanaka, Y. Li, G. Hirsch, R.J. Buenker, M. Kimura, H. Tawara, and Y. Nakai. *Phys. Rev. A*, 62:062715, 2000.
- [44] L.H. Toburen, M.Y. Nakai, and R.A. Langley. *Phys. Rev.*, 171:114, 1968.
- [45] S.L. Varghese, G. Bissinger, J.M. Joyce, and R. Laubert. *Nucl. Instrum. Methods*, 170:269, 1980.
- [46] G. Bissinger, J.M. Joyce, G. Lapicki, R. Laubert, and S.L. Varghese. *Phys. Rev. Lett.*, 49:318, 1982.
- [47] S.L. Varghese, G. Bissinger, J.M. Joyce, and R. Laubert. *Phys. Rev. A*, 31:2202, 1985.
- [48] S.L. Varghese. *Nucl. Instrum. Methods Phys. Res. B*, 24/25:40, 1987.
- [49] T.R. Dillingham, B.M. Doughty, J.M. Hall, T.N. Tipping, J.M. Sanders, and J.L. Shinpaugh. *Nucl. Instrum. Methods Phys. Res. B*, 40/41:40, 1989.
- [50] M. Horbatsch. *Phys. Lett. A*, 187:185, 1994.
- [51] M.B. Shah and H.B. Gilbody. *J. Phys. B: At. Mol. Opt. Phys.*, 14:2361, 1981.

- [52] C.F. Barnett, J.A. Ray, E. Ricci, M.I. Wilker, E.W. McDaniel, E.W. Thomas, and H.B. Gilbody. *Atomic Data for Controlled Fusion Research*, volume 1. 1977.
- [53] M.E. Galassi, P.N. Abufager, A.E. Martinez, R.D. Rivarola, and P.D. Fainstein. *J. Phys. B: At. Mol. Opt. Phys.*, 35:1727, 2002.
- [54] P.D. Fainstein, V.H. Ponce, and R.D. Rivarola. *J. Phys. B: At. Mol. Opt. Phys.*, 24:3091, 1991.
- [55] F. Blanco and G. García. *Phys. Lett. A*, 317:458, 2003.
- [56] Richard L. Liboff. *Introductory Quantum Mechanics*. Pearson Education Canada, 1992.
- [57] D. Pinchon and P.E. Hoggan. *J. Phys. A: Math. Theor.*, 40:1597, 2007.
- [58] W.J. Thompson. *Angular Momentum*. Wiley, 2008.